



Effects of post-processing operations on directed energy deposited 316 L stainless steel surfaces

Adriel Magalhães Souza¹ · Eraldo Jannone da Silva² · Hitomi Yamaguchi³

Received: 19 May 2023 / Accepted: 19 September 2023 / Published online: 11 October 2023
© The Author(s), under exclusive licence to Springer-Verlag London Ltd., part of Springer Nature 2023

Abstract

Directed energy deposition (DED) processes apply both material feedstock and energy for a layer-by-layer deposition, resulting in the formation of metallic parts. While DED excels in coatings, functionally graded materials, and repair, additional surface finishing is frequently needed in order to meet project requirements. This is usually due to low dimensional accuracy and poor surface quality. Chemopolishing, electropolishing, and abrasive processes (e.g., magnetic field-assisted finishing (MAF)) are fine-finishing operations that have been used for post-processing similar parts. Although most of these processes require their own specific processing equipment, MAF can be adapted to a machining center used for milling and grinding. This study involves a machining center and describes the investigation of process chains employing milling, grinding, and MAF for post-processing 316L stainless steel parts manufactured via DED. Parameters considered encompass shape deviation, roughness, microstructure, residual stress, material removal rate, processing time, cutting forces, and specific energy. Results show the post-process chain corrects surface errors without microstructure or hardness changes. Residual stress varies: milling leads to tensile stress, grinding leads to compressive stress, and MAF has minimal impact. Performing milling and grinding operations between DED and MAF minimizes polishing time. Furthermore, grinding reduces material removal in MAF, thereby decreasing the time required for polishing and overall specific energy consumption. This study also showed the feasibility of post-processing—from cutting to fine finishing—of DED parts using a machining center with one-time chucking. This concept will help save overall production time and improve part accuracy during post-AM processing.

Keywords Finishing · Additive manufacturing · Surface roughness · Milling · Grinding · Magnetic abrasive finishing

1 Introduction

AISI 316L stainless steel (SS) has been ubiquitously employed in the medical [1, 2], nuclear [3, 4], oil and gas [5], and food industries [6, 7] due to its inherent properties (e.g., corrosion resistance, mechanical properties, biocompatibility) [8, 9].

The material contains 66% Fe, 19% Cr, 9% Ni, 3% Mo, and 2% Mn with Si and C (the “L” in 316-L stands for low carbon content), and it is typically non-ferromagnetic [10]. Those characteristics make this alloy one of the most studied materials in metal additive manufacturing (AM) [11].

There have been significant advances during the last decades in the manufacturing technology for near net shape metallic component production through AM techniques [12]: powder bed fusion (PBF) and directed energy deposition (DED) standing out [13]. Both have similar manufacturing characteristics (metal added layer-by-layer); however, while thermal energy is applied in PBF for selective melting or fusion in certain regions of the powder bed, DED shows a combination of both material feedstock (powder or wire) and energy (i.e., laser) for the layer-by-layer deposition and, consequently, part formation [14]. PBF methods are more commonly used compared to DED, since PBF generates components with better tolerances while producing parts with greater geometric complexity [15]. Nevertheless,

✉ Adriel Magalhães Souza
adrielmagalhaes2@gmail.com

Eraldo Jannone da Silva
eraldodasilva@usp.br

Hitomi Yamaguchi
hitomiy@ufl.edu

¹ Department of Mechanical Engineering, São Carlos School of Engineering, University of São Paulo, São Paulo, Brazil

² Department of Production Engineering, São Carlos School of Engineering, University of São Paulo, São Paulo, Brazil

³ Department of Mechanical and Aerospace Engineering, University of Florida, Gainesville, FL, USA

DED technologies have been highlighted due to their applications such as coatings [16], functionally graded materials [17, 18], repairing or remanufacturing of damaged components [19, 20], and the possibility of adding features to preexisting parts [21]. Some advantages of DED are the potential for manufacturing directionally solidified [22] and single-crystal structures [23], microstructure control from changing process parameters and raw-material mixtures [24], and deposition of external layers with more noble material/mechanical properties than the substrate [25]. Despite the distinct features in AM technology (e.g., singular microstructures and properties due to their high cooling rates [26]), dimensional accuracy and surface quality are some of its critical limitations [27]. Therefore, additively manufactured (AMed) parts have a common need for post-processing operations (e.g., surface finishing methods, including material and non-material removal) in order to meet the strict performance requirements of high-end components, such as enhanced form accuracy and surface roughness.

Table 1 shows several post-process operations that are used for finishing AMed 316L SS components. For prismatic components, milling is a feasible option due to the efficiency of correcting geometric/dimensional errors and surface roughness reduction with a high material removal rate. Similarly, turning is a viable process for cylindrical parts. Grinding can be used as a finishing process on smooth surfaces with fine dimensional and geometric tolerances. The use of these methods in machining and turning centers is viable for post-processing external surfaces, including flat, cylindrical, and complex components (complexity is limited by the machine's degrees of freedom). Nevertheless, even with the implementation of auxiliary systems in the machines and the development of specific tools with high technological/economic demands, there is a technical limitation to post-processing when dealing with complex internal features, such as wiring conduits, micro-vanes, and conformal cooling channels.

Chemopolishing (CP) [52], electropolishing (EP) [39], and abrasive processes (e.g., magnetic field-assisted finishing (MAF) [28]) are fine-finishing operations that have been used for post-processing AMed parts. These procedures can generate components with textures ranging from sub-nanometer to micrometer scale, promoting surface functionalization (e.g., fluid flow, cell adhesion, wettability, corrosion resistance, among others). CP and EP processes chemically remove material, but MAF mechanically removes material through abrasives pressed against the target surface and equipped with magnetic tools suspended in a magnetic field, generating less hazardous waste. Moreover, MAF operations can be integrated in machine centers, eliminating the need for dedicated abrasive finishing setups, specific NC programs, or different workpiece fixtures for each process [58]. The polishing tool requires neither compensation nor dressing, with

self-adaptability and controllability, being additional advantages in MAF [59]. Nevertheless, low material removal rate (MRR) is one of the disadvantages.

Although it is possible to use abrasive processes such as a polishing step after DED due to the high initial roughness values (e.g., $R_a > 20 \mu\text{m}$ and $R_z > 100 \mu\text{m}$) and shape irregularities in the range of hundreds of micrometers, long post-processing times and high costs are required for achieving a surface roughness scales ranging from sub-nanometers to micrometers. In cases such as MAF, the process cannot correct geometric and dimensional errors because of the physical nature of the process (a pressure-copy operation). Therefore, an intermediate post-processing step between deposition and polishing may be necessary for correcting geometric and dimensional errors. Nevertheless, depending on the parameters and tools used, milling has a limitation when producing parts with a high-level surface finish (e.g., roughness at nanometer levels). Thus, adding abrasive processes such as grinding (bonded abrasives) and MAF (loose abrasives) when processing DED-produced metallic parts holds the potential to improve productivity and part quality. Despite this, each of those abrasive operations has limitations and technological challenges.

Regarding the scientific challenges posed by grinding, adequate dressing, cooling, and workpiece fixing device are fundamental for ensuring process efficiency. In regards to MAF, magnetic particle size, magnetic field, magnetic pole, rotation (cutting speed), and feed are essential variables that must be properly controlled for an effective process. Due to the nature of abrasive processes, the choice of abrasive type and size has a direct impact on the surface finish and must be carefully selected based on the workpiece material, desired material removal rate, and roughness. Accordingly, the development of some guidelines (based on technical criteria) can assist users in making appropriate decisions when determining strategies and optimal cutting conditions for these operations.

In the typical manufacturing sequence of metallic parts for medical applications such as 316L SS, the sequence often involves deposition (e.g., DED), followed by roughing and/or semi-finishing through milling and/or grinding. Nevertheless, the subsequent steps in manual polishing are not very productive and require a significant labor effort. Therefore, studies are needed to propose a manufacturing chain that eliminates or shortens these milling steps while reducing or eliminating the need for manual operations. One potential approach is to use a combined strategy that incorporates milling, grinding, and MAF. A significant productivity improvement and a reduced need for manual labor may be attained by this integrated approach in metallic medical device manufacturing. Table 2 provides a comprehensive summary of DED, milling, grinding, and MAF processes, elucidating the respective advantages and drawbacks asso-

Table 1 Overall comparison of surface post-process effect on the surface roughness of AMed 316L SS (or 316 SS)

Ref	Roughness in as-build state (μm)	Roughness after post-process (μm)	SRR** (%)	Post-processing time (min)	AM process	Post-process	Workpiece geometry
[28]	$R_z=102.1 \pm 3.8$	$R_z=0.13 \pm 0.07$	99.9	240	SLM	MAF	Flat
[29]	$R_a=8.8$	$R_a \approx 0.06^*$	99.3	-	SLM	μ M	
[30]	$R_a=9.69 \pm 2.52, R_z=64.86 \pm 15.03$	$R_a=0.07 \pm 0.01^*, R_z=0.6 \pm 0.15^*$	99.1, 93.3	-	SLM	SP-AD	
[31]	$S_a = 11.58$	$S_a = 0.14^*$	98.8	0.2	L-PBF	M	
[32]	$S_a = 1.74^{***}$	$S_a = 0.025$	98.6	-	SLM	SP-AD	
[33]	$R_a=14.75$	$R_a \approx 0.25$	98.3	-	SLM	G	
[34]	$R_a \approx 8$	$R_a = 0.18^*$	97.8	40	SLM	OECP+ECP	Flat, complex
[35]	$R_z = 80.6 \pm 19.6$	$R_z \approx 3^*$	96.3	105	SLM	MAF	Flat
[36]	$R_a=10$	$R_a=0.4$	96.0	-	SLM	T	Cylindrical
[40]	$R_a=10.63 \pm 2.02, R_z=62.38 \pm 10.81$	$R_a = 0.81 \pm 0.09^*, R_z = 4.96 \pm 0.45^*$	92.4, 92.0	32	L-PBF	MDIF	Cylindrical (Interior channel)
[32]	$S_a=15.76$	$S_a=1.74$	89.0	-	SLM	M	Flat
[41]	$R_a=9.27 \pm 2.03$	$R_a=1.11 \pm 0.06$	88.0	-	SLM	M	Flat, internal channel, cylindrical, conical
[42]	$S_a=10.99 \pm 1.27, S_z=128.65 \pm 15.47$	$S_a=1.39 \pm 0.47, S_z=9.81 \pm 2.15$	87.4, 92.4	0.6	L-PBF	M	Flat
[43]	$R_a \approx 23, R_z \approx 80$	$R_a \approx 3, R_z \approx 8^*$	87.0, 90.0	15	SLM	MAF	
[44]	$S_a=4.84$	$S_a=0.65$	86.6	-	L-PBF	LP	
[38]	$R_z=43 \pm 1$	$R_z \approx 6$	86.0	-	SLM	PG	
[42]	$S_a=10.99 \pm 1.27, S_z=128.65 \pm 15.47$	$S_a=1.98 \pm 0.95, S_z=17.14 \pm 4.15$	82.0, 86.7	0.06	L-PBF	G	
[45]	$S_a = 10.35 \pm 0.42$	$S_a = 1.92 \pm 0.11$	81.4	-	LMD	LP	Cylindrical
[46]	$R_a \approx 1.6, R_z \approx 9.9$	$R_a \approx 0.3^*, R_z \approx 2.5^*$	81.3, 74.7	-	SLM	UNSM	Flat
[47]	$R_a \approx 30$	$R_a=6.88^*$	77.1	15	SLM	USPee	
[48]	$R_a \approx 12, R_z \approx 72$	$R_a \approx 2.8^*, R_z \approx 20^*$	76.7, 72.2	75	SLM	MAF	
[49]	$R_a=6.6, R_z=35.7$	$R_a=1.6, R_z=9.2$	75.8, 74.2	-	DMLS	SPee	
[50]	$R_a=7 \pm 1$	$R_a=1.74$	75.1	-	SLM	T	Cylindrical

Table 1 continued

Ref	Roughness in as-build state (μm)	Roughness after post-process (μm)	SRR** (%)	Post-processing time (min)	AM process	Post-process	Workpiece geometry
[51]	$S_a=15.67\pm 3.25$	$S_a=4.51^*$	71.2	–	L-PBF	EMCP	Cylindrical (Interior channel)
[52]	$S_a=9.99, S_z=78.37$	$S_a=3.54^*, S_z=26.05^*$	64.5, 66.8	10	SLM	CPee+ECP	Lattice structure
[50]	$R_a=7\pm 2$	$R_a=2.7$	61.4	240	SLM	DF	Cylindrical
[53]	$S_a=10.2, S_z=157.3$	$S_a=5.5, S_z=75$	46.1, 52.3	12	PBF	EP	Flat
[50]	$R_a=7\pm 3$	$R_a=4.1$	41.4	–	SLM	VSF	Cylindrical
[40]	$R_a=10.63\pm 2.02, R_z=62.38\pm 10.82$	$R_a=6.32^*$	40.5	16	L-PBF	MAF	Cylindrical (Interior channel)
[53]	$S_a=10.2, S_z=157.4$	$S_a=8.8, S_z=147.2$	13.7, 6.4	180	PBF	TB	Flat
	$S_a=10.2, S_z=157.5$	$S_a=9.9, S_z=166.6$	2.9, +11.6	–	PBF	LP	Flat (internal)
[54]	$R_a\approx 20$	$S_a = 2.10 \pm 0.75, S_z = 44.50 \pm 13.45$	–	–	SLM	EP	Flat (internal)
		$S_a=13.88\pm 2.65, S_z=226.44\pm 17.68$	–	–	SLM	SB	Flat (internal)
		$S_a=5.22\pm 2.46, S_z=48.54\pm 21.41$	–	–	SLM	CP	Flat (internal)
[55]	–	$R_a\pm 0.27-0.52$	–	–	DED	M	Flat
[56]	–	$S_a\approx 0.8^*$	–	13	LMD	M	Flat
[57]	–	$R_z \approx 0.03^*$	–	–	PBF	μM	Flat

*Best condition

**Surface roughness reduction (SRR) (SRR=(initial-final roughness)/initial roughness)

***Milled surface. Abbreviations: SLM selective laser melting, L-PBF laser powder bed fusion, DED direct energy deposition, LMD laser metal deposition, DMLS direct metal laser sintering, MAF magnetic field-assisted finishing, μM micromilling, SP-AD surface polishing using abrasive disks, G grinding, OECF overpotential electrochemical polishing, ECP electrochemical polishing, T turning, SB sandblasting, TB tumbling, CFG creep feed grinding, EP electropolishing, MDIF magnetically driven internal finishing, M milling, LP laser polishing, PG pendulum grinding, UNSM ultrasonic nanocrystalline surface modification, USPe ultrasonic shot peening, SPe shot peening, EMCP electrochemical-mechanical combined polishing, CPee Cavitation peening, DF drag finishing, VSF vibratory surface finishing, CP chemopolishing. The (descending) order of presented post-processing operations is based on their capability of SRR

Table 2 Summary of DED, milling, grinding, and MAF processes and the main contributions/limitations of this study

	Process	Main comments	Strengths	Weakness
Overall	DED	Selection of parameters to ensure productive production of parts with favorable geometry and mechanical performance	3D Near Net Shape components	Dimensional tolerance and surface finish
	Milling	Operation is versatile (different types of cutters are applicable for the fabrication of different specimen geometries and materials)	Efficiency of correcting dimensional errors and surface roughness reduction with a high material removal rate	Milling marks on the surface, which can compromise the functionality and lifespan of the part
	Grinding	The use small diameter grinding (under explored in the existing literature) wheels may be potential substitutes or complements to milling operations in machining centers	Grinding can be used as a final machining process to produce components with smooth surfaces and fine tolerances and to remove milling mark	The implementation of peripheral and auxiliary systems in the machine are necessary to achieve the desired efficiency
	MAF	Process can be integrated in machine centers, eliminating the need for dedicated abrasive finishing setups	The milling/grinding marks can be smoothed, and the surface quality improved	High level of specific energy and less material removal compared to milling and grinding
Main contributions of this study		<p>A combined strategy that incorporates milling, grinding, and MAF</p> <p>The exploration of use of small diameter tools for grinding in machining centers</p> <p>Integration of MAF operation into a machine center, replacing manual polishing operations</p> <p>The viability of post-processing—from cutting to fine finishing—of DED parts using machining centers</p> <p>The feasibility of high-speed MAF</p>		
Limitations of this study		<p>As a fundamental study, only flat surfaces were studied</p> <p>Due to technological-economic constraints, exclusive use of static dressing prevented modifying superabrasive electroplated quill surfaces, leading to a detrimental impact on ground part surface quality</p>		

ciated with each technique. Furthermore, it outlines the principal findings and constraints of this study.

The post-processing chain needs to be selected based on the desired MRR, surface geometry (form accuracy, surface roughness, and texture), and other design parameters. Although milling is an effective method for correcting geometrical errors on the surface, marks which can compromise the functionality and lifespan of the machined part are inevitable. Grinding as an intermediate post-processing step after milling may improve surface quality. Also, the use of small-diameter grinding wheels, whether conventional or superabrasive, may be potential substitutes or complements to milling operations in machining centers. Thus, this study will discuss the use of small-diameter tools for grinding in machining centers. This approach aims to replace rough and finish milling procedures with abrasive tools, thus allowing rough and semi-finishing processes to be performed in machining centers with an abrasive tool and fine finishing to be performed with the MAF process. High-speed polishing can be another alternative for desired surface characteristics.

Nevertheless, the impacts on the surface and limitations of each post-processing step should be better clarified in the process chain of AMed metallic parts.

This study involves a machining center and describes the investigation of process chains employing milling, grinding, and MAF for post-processing 316L stainless steel parts made through DED. A combined strategy of post-processes was studied for finishing flat components in sequence, with shape deviation, surface roughness, microstructure, residual stress, and MRR as evaluated parameters. Processing time and specific energy were measured and analyzed for each process chain. This manuscript is organized as follows: Sect. 2 presents the development of the post-processing sequence in machining operations (milling, grinding, and MAF) performed in a high-speed machining center—the capabilities and limitations of each operation are presented. Section 3 reports the methodology that was applied. Results are presented in Sect. 4 and discussed. Finally, Sect. 5 provides conclusions.

2 Post-processing AMed DED parts by machining

This section is divided into two subsections. The first subsection discusses various prospective post-processing alternatives along with their respective advantages and limitations. It also entails the presentation and discussion of outcomes from exploratory grinding and milling experiments conducted on machining centers. The subsequent subsection outlines the approach employed to incorporate the MAF process into machining centers.

2.1 Possible post-DED processing operations in machining centers

A trade-off between processing conditions and part quality has driven AM machine-tool manufactures to improve AM equipment. A common process chain includes milling after DED in order to correct dimensional and geometrical errors. As such, machine-tool manufacturers have incorporated AM capabilities into three and five-axis machining centers [60–62]. Machining centers combining DED with other machining/polishing processes can be used to repair high-value-added tooling parts, build functionally graded materials, and control geometric accuracy, among other corrections. This led to users being challenged to design effective AM processing conditions and post-AM process chains that enable the delivery of AM parts. If a DED-produced part requires a smoothly finished surface, the part needs to be included in a finishing stage. An alternative is the use of abrasive finishing technologies, such as grinding and/or polishing after milling. Those processes require additional equipment such as grinders and dedicated abrasive finishing setups. Not only does the additional equipment and processing lead to increasing production costs, extended processing times, and added labor costs, but the part accuracy is also impacted by moving the part for the required processing. Full knowledge of the post-processing impacts on the workpiece is required for designing a process chain that maximizes its advantages while minimizing its limitations.

Figure 1 shows a flowchart of possible post-processing alternatives for producing mirror-like surfaces. Due to the particularities of the AM process and conditions, each process will deliver the part with a certain degree of roughness changing from few microns to hundreds. The low surface and dimensional quality of AMed parts may be associated

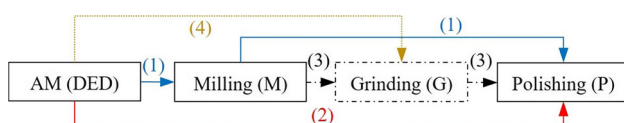


Fig. 1 Flowchart of possible post-DED process operations

with several factors, such as deposition bead morphology/geometry, balling phenomenon (liquid material does not adhere to the adjacent substrate because of surface tension), or presence of semi-fused powders adhered to the surface [63, 64]. Regarding AM, the parameters must be chosen as adequately as possible in order to avoid internal defects (e.g., porosity), imperfections (e.g., heterogeneity in mechanical properties), and lamination while maintaining fair productivity. After deposition, geometric and dimensional deviations and surface roughness should be minimal. In such cases, less post-processing time is required to increase the part's surface quality and dimensional accuracy. Traditionally, milling followed by polishing (Route 1) or milling followed by both grinding and polishing (Route 2) can smooth the part's surface while providing sufficiently high form accuracy for prismatic components. Despite milling operations being versatile, different types of cutters are applicable for manufacturing different specimen geometries and materials, where productivity and part quality are affected by experimental conditions, and the milled surface shows visible cutting marks, which are intrinsic to the process. Route 3 includes only grinding. Although grinding is traditionally an operation for the final finishing of components [65], its effectiveness is deeply linked to the grinding conditions, grinding wheel, and its conditioning (dressing) [66]. In some cases, the implementation of peripheral and auxiliary systems are necessary in order to achieve the desired efficiency in the machinery. These may vary from monitoring (e.g., acoustic emission), to fixing, cooling, balancing, and dress systems, as well as the development of new grinding wheels—all of these demanding high technological and economic resources. The main disadvantage of Route 3 is the lower material removal rate of grinding compared to milling. Both operations are performed in machining centers; superabrasive electroplated quills can be used as alternatives for increased material removal rate, but there is a significant impact on roughness. Polishing parts right after AM (DED) (Route 4) is a costly, time-consuming, and uncommon practice as the printed surface roughness values need to be reduced to sub-micrometer scales, depending on component application. Several polishing processes can be used (e.g., CP, EP, MAF), and a roughness reduction of up to 99.9% may be achieved with the application of polishing as post-process, depending on the quality of the part received from AM and the desired final characteristics (i.e., roughness at nanometric levels). Nevertheless, a long processing time is required for such reduction (up to 4h). Although polishing can smooth surfaces from nano-to-sub-micrometer scale, an intermediate post-processing step between deposition and polishing may be necessary for correcting geometric and dimensional errors while shortening the polishing time needed to reach target surface roughness values.

In this research, a series of experiments were conducted using a three-axis CNC machine center (Hermle, C800U—

German machine) in order to explore the grinding process using small-diameter wheels in machining centers. Vertical spindle surface and tangential grinding tests were analyzed with different types of grinding wheels made of diamond (referred to as *D*), cubic boron nitride (cBN—referred to as *B*), and alumina (Al_2O_3 —referred to as *A*). Several grinding conditions were evaluated, where the grinding parameters were determined based on the manufacturers' recommendations. Spindle rotation ranged from 4000 to 15,000 rpm, which allowed a cutting speed between 4 and 45 m/s. The feed ranged from 5 to 1000 mm/min. Depth of cut varied between 5 and 30 μm . Figure 2 shows the surface roughness after the DED-316L SS grinding post-processes. Using superabrasive electroplated quills (tools 1–3 used in a lateral configuration), the final roughness was around 4 μm R_a . Such high values can be justified by the geometry of the tools, grain distribution via the electroplating process, grain size (equivalent to 150–180 μm), and inability to dress by single-point dressers. Although the superabrasive grinding wheel has a high material removal capacity, it is not recommended to be dressed by static dressers, which negatively affect roughness. This dressing limitation can be overcome through conventional wheels, thus impacting cutting ability and final roughness. The use of tools in a vertical configuration (surface grinding) generated parts with lower roughness compared to a lateral configuration. Thus, cup-type grinding wheels were used, which can be found in manufacturers' inventories due to their common utilization in the industry for sharpening steel tools. Consequently, this variant of grinding wheel stands as a plausible alternative for implementation within machining centers (3 to 5 axes). These centers necessitate the fabrication of both a rod and a flange to facilitate coupling with the mandrel and the machine shaft. The electroplated diamond grinding wheel (tool 6) provided better surface quality to the parts compared to the other electroplated tools, with roughness levels close to 0.3 μm R_a . However, as this wheel is

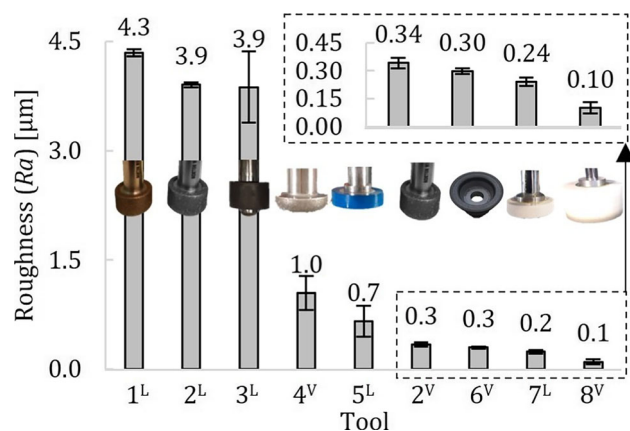


Fig. 2 Surface roughness after different grinding post-processes of DEDed 316L SS

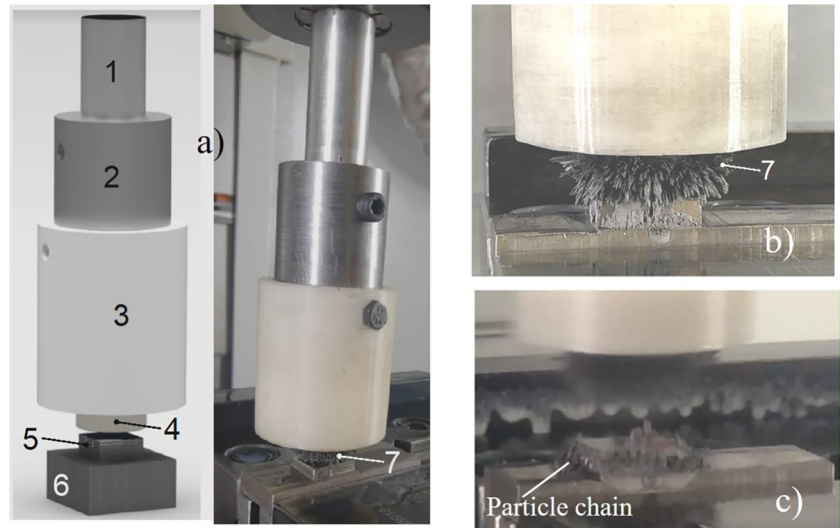
electroplated superabrasive, dressing with static tools (e.g., single-point dressers) is still a limitation for its application (as previously discussed). Final roughness was around 0.1 μm R_a though tool number 8 in a vertical configuration. Such a level can be justified by a combination of factors, such as tool geometry (cup-type grinding wheel), grain size, and dressing capacity by single-point dressers. Thus, a series of grinding experiments was carried out to explore the possibility of conducting this process in machining centers. Depending on the process parameters, especially the tool's specifications and its surface condition, the resulting roughness values are quite varied, ranging from 4 to 0.1 μm R_a . It is up to the operator to define which grinding wheel and condition should be used, depending on the technical criteria of the project. Some guidelines explored and defined by the tests can help in decision-making, such as defining the abrasive grain (type and size), binder, tool geometry, orientation (vertical or lateral configuration), grinding parameters, and dressing.

Grinding is rarely adopted after building a part through AM. Directed deposited energy (DEDed) metallic components do not have tight dimensional and geometrical tolerances to match practical requirements, and errors can range up to 300 μm . This will require multiple grinding passes for corrections, which can be costly and time-consuming (Route 3—Fig. 1), as the depths of cut are limited to micrometer ranges. An intermediate post-processing operation (e.g., milling) between the deposition and grinding process may be necessary in order to overcome this challenge (Route 2—Fig. 1), adopting depths of cut at millimeter ranges. In such cases, grinding can be used as a final machining process in order to produce components with smooth surfaces and fine tolerances, as well as removing milling marks. Vertical spindle grinding in machining centers will require the implementation of auxiliary systems for dressing the wheel, either through static tools or rotatory dressers in the case of superabrasive wheels. Regarding the use of cutting fluid, pumps installed in machining centers are usually less powerful than those industrially commercialized in dedicated grinder machines. Therefore, if the coolant system (pump/nozzle) is not efficient, it can result in greater thermal damage to the ground component.

After defining the most suitable grinding wheel to be used in the proposed process chain, the subsequent step is the determination of the milling conditions based on the selected tool material and geometry.

Milling experiments were carried out using the Hermle C800U German machine center in order to explore their DEDed 316L SS post-processing capacity. A 20-mm diameter end-mill tool (R390-11 T3 08 M-PM 1030 insert code) was used for milling. Milling conditions were determined based on the manufacturers' recommendations, which were spindle rotation (n), 4215; cutting speed (v_c), 265 m/min (4.4 m/s); depth of cut (a_p), 0.4 mm; and feed per tooth (f_z),

Fig. 3 Detailed of the developed MAF tool



0.08, 0.12, and 0.2 mm/tooth (referred to as M1, M2, and M3, respectively). The a_p used for milling was 0.4 mm, forty times greater than the one recommended for grinding. Although milled parts have reached low roughness values (0.2–0.3 $\mu\text{m } R_a$), the surface features periodic tool marks.

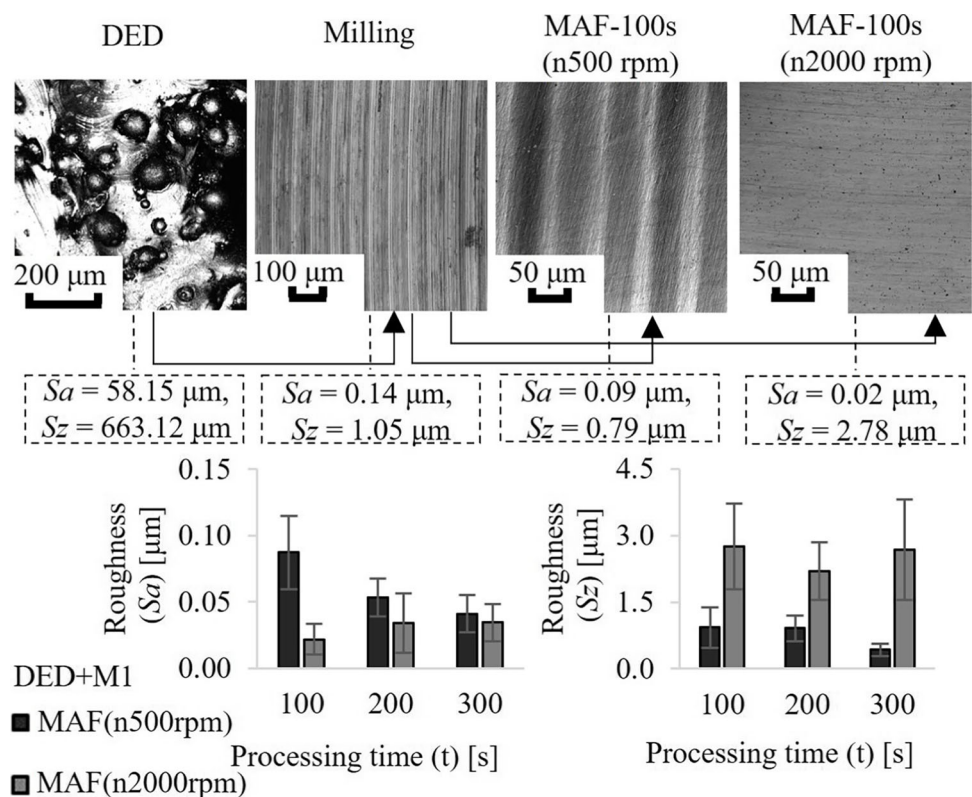
Considering that this study also tends to contribute to the definition of processes, tools, and favorable conditions for 316LSS components production at micro/nanometric roughness levels, as well as the most suitable grinding wheel and

end-mill tool, the next step is the development of the polishing tool.

2.2 Integration of MAF in machining center

The next step in the development of the proposed process chain for DED parts was the integration of fine-finishing operations in a machining center. Magnetic abrasive finishing (MAF) has shown the ability to smooth AMed part surfaces by means of an abrasive pressed by a flexible iron-particle

Fig. 4 Surface topographies after different post-processes and influence of spindle rotation on surface roughness over polishing time



brush in a magnetic field [67]. MAF has been incorporated in a machining center by simply exchanging the cutting tool with a tool consisting of permanent magnets that suspend the particle brush [68]. As such, it may be useful to combine MAF and DED in a single machining center.

Figure 3 shows a tool consisting of permanent magnets developed for incorporating MAF in a machining center (Hermle C800U was used to carry out the tests). Three magnets ($\varnothing 22 \times 10$ mm) were coupled inside a polylactic acid (PLA) case, with the case preventing the magnets from oscillating during polishing at high rotational speeds. This tool was assembled into the machining center. A mixture of magnetic particles and abrasives was attached to the magnet and formed a particle brush along the magnetic field lines. The measured magnet flux density at the magnet center was 544 mT.

Reducing polishing time is a key strategy of combined post-DED processing. Prior to fully implementing MAF in a post-DED process chain, the feasibility of high-speed MAF was tested using a DED sample with a milled surface. Surface topographies of the sample centers after each processing step are shown in Fig. 4. While milling marks were still visible after polishing with a spindle speed of 500 rpm, the smoothed surface was free of milling marks when using a spindle speed of 2000 rpm. Translating the particle brush over the surface at faster speeds enabled more material to be removed in a shorter time, but the aggressive contact of the particle brush facilitated the creation of pits on the polished surface, increasing the roughness S_z . Those pits can also be associated with defects arising from the deposition process.

Figure 5 shows the surface topographies after 300 s. Both cases produced a smoothly finished surface at the center of the workpiece. Nevertheless, the workpiece edges were not fully polished in either case, and the unpolished region was wider

at a spindle speed of 2000 rpm when compared to 500 rpm. This can be associated with the “edge effect” (different magnetic flux density at the center and edge of the magnet) and the rotational movement of the magnetic brush (different cutting force at the center and edge of the magnet due to relative velocity and centrifugal force in circular motion) [69]. Under these conditions, magnet diameter ($\varnothing 22$ mm) was greater than the workpiece surface area (15 L \times 20 W mm). Once the magnet neared the workpiece, some particles—especially those located near the area corresponding to outside the workpiece—were attracted by the steel substrate and formed particle chains with the steel substrate rather than rotating with the magnet, as shown in Fig. 3c. As a result, the polished area was reduced only because particles near the inner region of the magnet participated in the polishing action. This trend was more obvious at higher spindle rotational speeds. As such, it was concluded that increasing spindle speed leads to an increased material removal rate, but reduced polished area.

To realize high-speed MAF, the magnetic field that controls the particle-brush behavior must be modified in order to satisfy the following requirements:

1. Focus the magnetic field toward the target surface area.
2. Avoid direct contact of the particle brush with the steel substrate to prevent particle-brush breakup.

A pole tip (1020 steel, $\varnothing 12 \times 5$ mm) (the end face is smaller than the target area) was attached to the magnets in order to satisfy the first requirement. As for the second requirement, aluminum dummy blocks were placed beside the workpiece in order to disrupt the direct contact of the particle brush with the steel substrate without disturbing the magnetic field

Fig. 5 Micrographs of workpiece surface after polishing

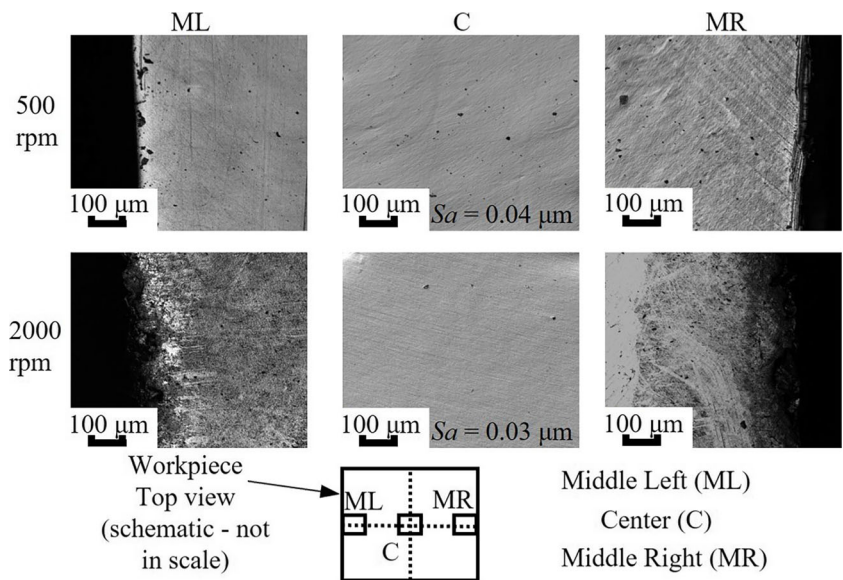


Table 3 DED conditions

Material (chemical composition - wt.%)	316L SS (18.1 Cr; 14.4 Ni; 2.4 Mo; 0.6 Si; <0.05 V, C, Nb, Cu, Ti, P, Al, S; Bal. Fe)
Workpiece	$15 \times 20 \times 8 \text{ mm}^3$, $12 \times 12 \times 8 \text{ mm}^3$ 316L SS (after DED: $15.15 \pm 2.96 \mu\text{m } R_a$, $105.39 \pm 12.39 \mu R_z$, $0.49 \pm 0.46 R_{sk}$, $3.84 \pm 1.30 R_{ku}$, $160.45 \pm 22.49 \mu P_t$)
DED	
Machine	BeAM (manufacturer based in France)-Modulo 250 (5 axis)
Laser	Continuous Nd:YAG (1070 nm), 0.75 mm laser spot diameter, 350 W
Powder	Feeder: disk groove (1.3 mm depth and 15 mm width), 6.5 g/min powder flow rate
Deposition strategy	Zig-zag (90° rotation among the layers)
Protective gas	Argon (3L/min nozzle and carrier gases, 6L/min shield gas)
Focal distance	3.5 mm
Overlapping (Δx)	0.25 mm
Layer height (Δz)	0.2 mm
Feed rate (v_f)	2000 mm/min
Referred to as	DED

at the polishing area. The efficacy of these modifications on the particle-brush behavior at increased spindle speeds (~ 6000 rpm) was tested by a particle-brush-stability test. New workpieces were deposited with dimensions equal to $12L \times 12W \times 8H$ mm. Thus, all particles formed a particle brush that covered the polished area. Increasing the spindle speed created greater centrifugal force on the particles. This caused two major effects in the particle-brush formation: a funneling effect near the pole tip and an enlargement

of the particle-brush diameter, some of which slides along the sides of the sample. As a result, fewer particles engaged with the workpiece surface, thus diminishing polishing performance. These trends are more obvious above spindle speeds of 4000 rpm. Beyond this value, the tool also showed wobbling motion, which could be caused by eccentricity in the system. As such, a spindle speed of 2000 rpm was chosen for MAF in this study.

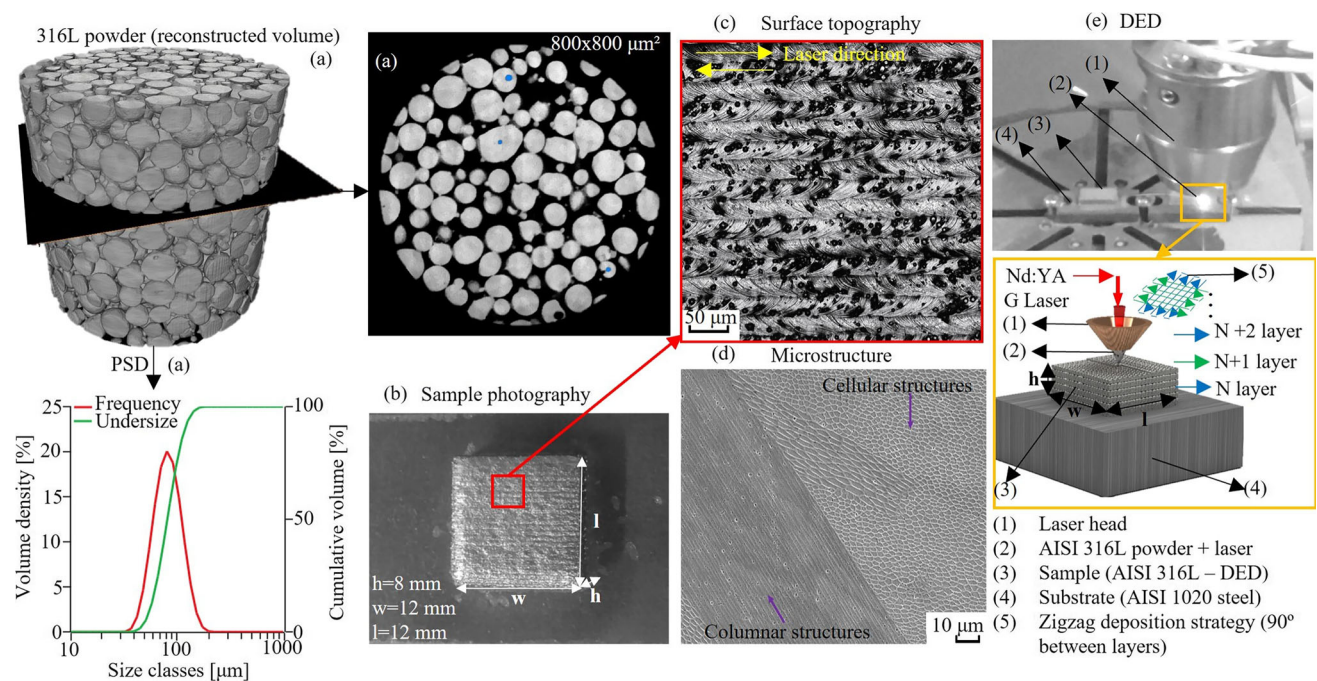


Fig. 6 a 316L SS powder (reconstructed volume and PSD), b representative part, c surface topography, d microstructure, and e schematic of part-fabrication process using DED

After defining the most suitable tools and their conditions, the subsequent step was the evaluation of each post-process on surface finishing characteristics. Material removal rate, processing time, and specific energy were also evaluated.

3 Experimental procedures

The initial segment of this section pertains to the materials and methods employed for DED deposition. Subsequently, the tools and parameters utilized in the milling, grinding, and MAF processes are elucidated. Concluding this portion, the approach taken to analyze force, specific energy, and surface characteristics (e.g., shape deviation, roughness, microstructure, hardness, and residual stress) will be delineated.

3.1 Additive manufacturing: powder properties and DED parameters

Table 3 shows the chemical composition of the gas atomized 316L SS powder provided by LPW Technology (investigated by spark optical emission spectrometry (S-OES)—Anacom Scientific, B2ADV, equipment manufactured in Brazil). Particle-size distribution (PSD) of the powder, predominantly spherical, is between 40 and 120 μm —sieve analysis: $D_v(10) = 57 \mu\text{m}$, $D_v(50) = 82 \mu\text{m}$, and $D_v(90) = 119 \mu\text{m}$ (see Fig. 6a). Powder/sample porosity was investigated by X-ray computed microtomography ($\mu\text{-CT}$) (Zeiss Xradia Versa XRM-510—American equipment, 0.80 μm pixel size, filter HE#1, 1000 views) with 10 W at 160 kV. The powder’s feedstock internal porosity (before deposition) and samples (after DED) are 0.07% and 0.00003%, respectively. The powder was dried prior to DED (1 h, 110 $^\circ\text{C}$). Samples were manufactured with $15 \times 20 \times 8 \text{ mm}^3$ and $12 \times 12 \times 8 \text{ mm}^3$ (Fig. 6b) using the parameters listed in Table 3. Figure 6c and d show the surface topography and microstructure after DED. A zig-zag deposition strategy with 90° rotation among the layers was adopted, and a schematic part-fabrication process can be seen in Fig. 6e.

3.2 Milling, grinding, and MAF conditions

The milling, grinding, and MAF processes were selected to be part of the proposed process chain for mirror-like surface part production by AM through DED technology. The machining experiments were carried out using a three-axis CNC machine center (Hemle, C800U—German machine). Table 4 shows the operational conditions. Milling and grinding conditions were determined based on the manufacturers’ recommendations and preliminary tests (see Sect. 2). A 20-mm diameter end-mill tool (R390-11 T3 08M-PM 1030 insert code) was used for milling (same tool reported in Sect. 2.1). A straight cup grinding wheel (101.60×50.80×31.75 mm, ACR FE 38A80 k) was used on a vertical spindle surface configuration for grinding. The choice of this grinding wheel was due to the lowest roughness achieved among the tested tools and is reported in Sect. 2.1—see Fig. 2, tool 8. Before the grinding experiments, this grinding wheel was dressed with a single-point stationary dresser, adopting the following parameters: 32 dressing overlap ratio (U_d), 10 μm dressing depth (a_d), 6000 rpm rotation (n)—which allowed a cutting speed of approximately 32 m/s, 150 mm/min traverse rate (v_t), and 0.025 mm/rot crossfeed (S_d). These parameters were defined through preliminary tests in order to minimize the roughness of the part. During the milling and grinding tests, an ester-based semi-synthetic fluid was used with a 42 L/min flow rate and a concentration of 6%. For MAF, the tool developed in Sect. 2.2 was adopted, having alumina abrasive (1 μm mean size; 0.1 g), iron particles (60 μm mean size; 0.9 g), and hydraulic oil (Hydra XP 32; 0.4 mL). The measured magnet flux density at the pole tip center was 428 mT. The feed rates in MAF were the same as those adopted in M1 milling condition ($v_f=1012 \text{ mm/min}$) and G1 grinding condition ($v_f=200 \text{ mm/min}$), respectively. The iron particles were replaced in the end of each polishing test (after 90 passes with a 1012 mm/min feed rate and 36 passes with a 200 mm/min feed rate). After each measurement, 0.1 mL of slurry (mixture of abrasive and oil) was added to the flexible brush.

Table 4 Operational conditions for milling, grinding, and MAF

	Milling		Grinding	MAF	
n (rpm)	4218		3000	2000	
v_c (m/min) [m/s]	265 [4.4]		958 [15.9]	-	
a_p (mm)	0.4		0.01	-	
f_z (mm/tooth)	0.08	0.2	-	-	
Workpiece-pole	-	-	-	2	
Tip clearance (mm)					
Magnet feed (mm)	-	-	-	24 mm	
v_f (mm/min)	1012	2531	200	200	1012
Process name	M1	M3	G1	MAF(Vf200)	MAF(Vf1012)

3.3 Force, specific energy, shape deviation/roughness measurements, metallographic preparations, microhardness, and residual stress measurements

A piezoelectric dynamometer (Kistler, type 9257BA - Swiss equipment) with a 2 kHz sampling frequency was used for measuring the radial force (F_r), feed force (F_f), and axial force (F_a) during processing. It selected measurement ranges of ± 0.5 kN in the X- and Y-directions and ± 1 kN in the Z-direction. Measured force data were used to calculate the specific energy (u) for each machining process, according to Eq. 1:

$$u_{M,G,MAF} = \frac{F_c \cdot v_c}{MRR} \quad (1)$$

where F_c is the cutting force, v_c is the cutting speed, and material removal rate (MRR) is the volume of removed material (V_{rem}) divided by the processing time (t_c). V_{rem} was calculated by the difference in mass (before and after post-processing) divided by material density— 8 gcm^{-3} [70]. Material removal was measured using a precision scale (0.1 mg resolution, JINGHUA Instruments, FA2104N—Chinese equipment).

The specific energy for DED (or volumetric energy density) was calculated according to Eq. 2 [71]:

$$u_{DED} = \frac{P}{v_f \cdot d \cdot h} \quad (2)$$

where P is the laser power, v_f is the feed rate (deposition speed), d is the laser diameter, and h is the layer thickness. The u_{DED} represents the total energy absorbed by the molten pool during deposition [71].

A relationship between specific energy and equivalent chip thickness (h_{eq}) for each post-process was created. Although chip thickness in milling varies according to the rotational angle of the tool, the h_{eq} for milling is based on

Woxén's fundamental conditions, which can be calculated, as a simplified version, according to Eq. 3 [72]:

$$h_{eq-M} = \frac{A}{l_c} \quad (3)$$

where A is the chip area and l_c is the active cutting edge length.

Regarding grinding and MAF, the h_{eq} values were calculated according to Eq. 4:

$$h_{eq-G,MAF} = \frac{MRR}{b \cdot v_c} \quad (4)$$

where b is the width of cut and v_c is the cutting speed.

The shape deviation (primary profiles, P_t —total height) was measured using a stylus-roughness tester (Taylor Hobson, Talysurf 50—Britain equipment). Directions parallel and perpendicular to the feed/build direction were analyzed. Five parallel profile lines (with a 2 mm gap between each one) were evaluated (10 mm evaluation length). A wide range gauge (ruby ball point with $500 \mu\text{m}$ tip radius) was used to measure form deviation.

The same stylus-roughness tester described above was used to measure surface roughness. The contact stylus sensor (pick-up) was changed to the one suitable for measuring roughness, and a diamond inductive conisphere point with a $2 \mu\text{m}$ tip radius gauge was used. Five parallel profile lines (4 mm evaluation length for milled/ground/MAF samples) were evaluated and averaged for roughness measurements. Regarding the roughness of DEDed samples, scans were taken with a magnification of ten and stitched together, resulting in a total evaluation area of $3831 \times 3837 \mu\text{m}^2$.

The topographies and 3D surfaces were characterized with a confocal microscope (Olympus LEXT 4100—American equipment). After each process, the samples were ultrasonically cleaned (in isopropyl alcohol for 10 min) for mass loss, shape deviation, and roughness measurements. Metallographic investigations were performed through a scanning electron microscope (JEOL IT-200—American equipment). Samples were cut using wire electrical discharge machin-

Fig. 7 Scheme of residual stress measurement **a** and principal stress and strain directions **b**

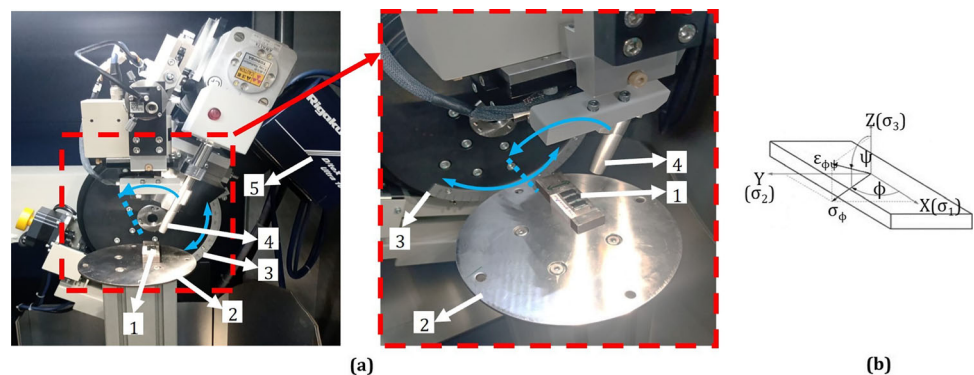
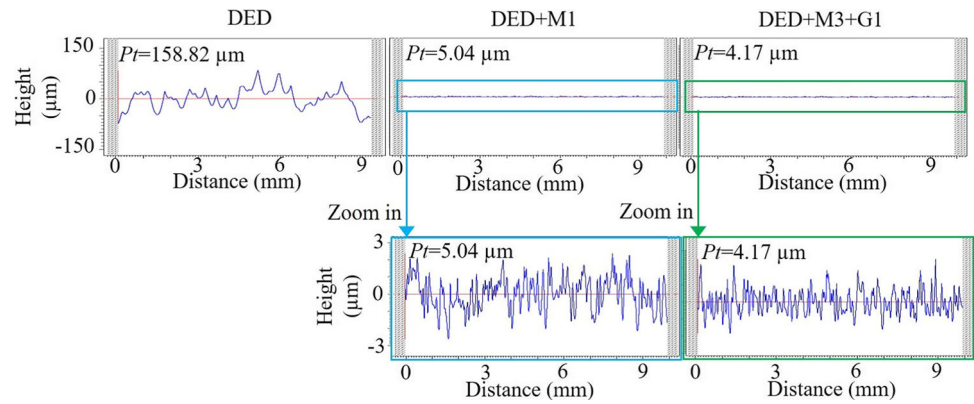


Fig. 8 Primary profile after DED, DED+milling (M1) and DED+milling(M3)+grinding (G1)



ing (WEDM), inlaid in Bakelite, sanded, polished, and electrolytically etched with oxalic acid (H₂C₂O₄). Vickers microhardness tests were performed with a hardness tester (Buehler Model 1600 6300—Canadian equipment) following the ASTM E384 standard [73], a 0.5 N load, and 15 s dwell time. Indentations were made from 50 μm of the post-processed surfaces up to 250 μm (in a 50 μm interval). The indicated hardness values correspond to the arithmetic mean of the 60 measured values.

An X-ray diffractometer (Rigaku brand, model Automate II—Japanese equipment) was used for residual stress (RS) measurements, working at 20 mA and 10 kV with a radiation source of chromium (Cr) with a K α filter of vanadium—wavelength (λ) equal to 229 nm [74]. The samples were positioned horizontally (referred to as 0° - transverse to feed direction) and vertically (referred to as 90° - same feed direction) in the equipment. Figure 7a shows the schematic configuration of the RS measurements. No surface preparation was applied prior to measurements as to check RSs on the top surface layer after each respective process. The sin² (ψ) method was adopted with 7 ψ angles between 0 and 60°— ψ being the inclination of the diffraction plane and the plane of the sample—polar or zenith angle in the spherical coordinate system, according to Fig. 7b. The scan ranges (2 θ) varied between 126–132° and 118.84–139.04°, with a sampling width of 0.04° and 0.1°, respectively. The austenite peak 220 was set for the diffraction peak. The ISO-inclination method was used for measurement, using a Savitzky-Golay filter for smoothing. The adopted Young’s modulus (E) and Poisson’s ratio (ν) were 200 GPa and 0.29, respectively.

4 Results and discussion

To begin, the section will outline the repercussions of the operations on the surface characteristics of the samples, including shape deviation, roughness, microstructure, and residual stress. Subsequently, attention will shift toward an analysis of key process output parameters, including material removal rate, processing time, and specific energy consumption.

4.1 Surface finishing characteristics

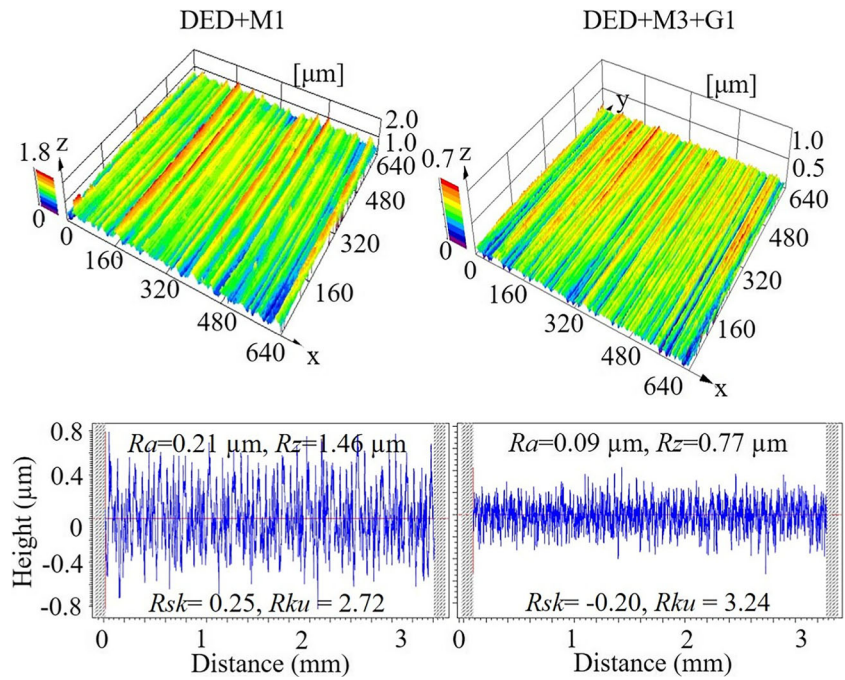
Figure 8 shows the primary profiles of DEDed, milled (DED+M1), and ground surfaces (DED+M3+G1). Table 5 shows the geometric deviation (P_t) results after each process. The values after MAF are statistically similar to the values from the previous post-process, as MAF does not change straightness (a pressure-copying process does not correct geometric errors). There is no significant difference between the P_t values measured in the direction parallel and perpendicular to the feed/build direction. High straightness errors were found for parts after DED due to AM process characteristics (e.g., deposition beads morphology and geometry). The results suggest that a minimum offset for machining should be near 0.2 mm for correcting geometric and dimensional errors. After three milling passes ($a_p=0.4$ mm), geometric deviations from the DED were completely removed (the initial value of 160 μm was reduced to around 5 μm P_t). Due to the higher level of precision during the finishing of the work-piece, the ground surfaces were straighter (4 μm P_t) than the milled surfaces. Moreover, the standard deviation for ground

Table 5 Straightness of surface in μm after each post-process

Process	DED	DED+milling	DED+milling+grinding	DED+milling+MAF*	DED+milling+grinding+MAF*
Global mean	160.45	5.23	4.20	5.20	4.22
Std. dev	±22.49 (14%)	±0.67 (13%)	±0.36 (9%)	±0.66 (13%)	±0.41 (9%)

*Average between 200 and 1012 mm/min

Fig. 9 Initial surface condition after milling (M1) and grinding (G1)

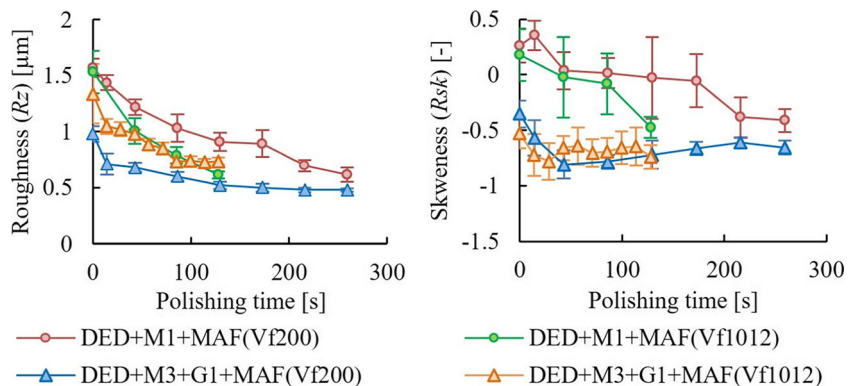


surfaces is the lowest (9%), showing good process repeatability.

Figure 9 shows the surface topographies after two process-chain sequences: (a) DED + milling (M1) and (b) DED + milling (M3) + grinding (G1). The intent was to produce a smoother surface for the MAF process in a shorter machining time. The roughness parameters R_{sk} and R_{ku} are used to characterize the surface roughness distribution, providing additional information about the shape and concentration of irregularities. These parameters describe surface features that the R_a and R_z values do not capture. Therefore, a combination of different parameters (R_a , R_z , R_{sk} , and R_{ku}) has been presented to obtain a more comprehensive understanding of the surface characteristics. The surface profile after milling (M1) had periodic marks resulting from the milling operation ($f_z=0.08$ mm/tooth; $a_p=0.4$ mm). The profile after grinding (G1) also had some periodicity due to the random characteristic of the abrasive tool’s cutting edges and the conditions used

($f=0.067$ mm/rev; $a_p=0.010$ mm). The milled surface was rougher than the ground surface. The initial roughness values (15.15 ± 2.96 μm R_a , 105.39 ± 12.39 μm R_z after DED) were reduced in 2.1 s to 0.21 ± 0.02 μm R_a and 1.55 ± 0.14 μm R_z after milling (M1) and in 10.8 s to 0.13 ± 0.03 μm R_a and 1.16 ± 0.26 μm R_z after grinding (G1). The high DED surface roughness values may be linked to several factors, such as deposition bead morphology, the geometry balling phenomenon (liquid material does not adhere to the adjacent substrate because of surface tension), and the presence of non-fused powders adhered to the surface. A 99% surface roughness improvement was achieved in approximately 12 s of post-processing time with milling (DED+M1) and grinding (DED+M3+G1) as post-processes. A positive skewness was obtained for milled surface (M1= 0.22 ± 0.19 R_{sk}), while negative skewness was obtained for the ground surface (G1= -0.44 ± 0.15 R_{sk}). Milled (DED+M1) and ground (DED+M3+G1) surfaces were polished with MAF with

Fig. 10 Impact of magnet feed rate and number of passes during MAF on surface roughness of M1 and G1 samples



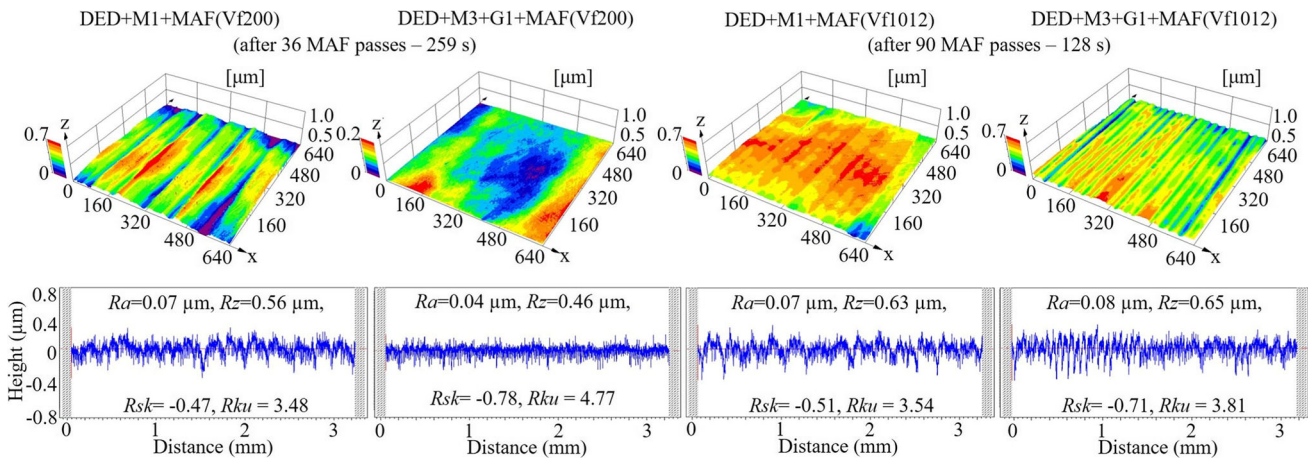


Fig. 11 Impact of magnet feed rate and number of passes during MAF on surface topography of M1 and G1 samples

different magnet feed rate: conditions MAF(Vf200) and MAF(Vf1012), in 259 and 128 s, respectively. The polishing experiments were performed until the surface roughness reached around $0.6 \mu\text{m } R_z$ ($\sim 0.07 \mu\text{m } R_a$), which seems to be the characteristic roughness for the conditions used in this study. Those roughness limits were investigated after polishing of milled samples (DED+M2). Ninety MAF passes were performed using a feed rate of 200 mm/min (roughness was measured at every 30 passes). Roughness reached the limit after 30 passes (~ 260 s polishing time).

Figure 10 shows the changes in roughness R_z and skewness R_{sk} with polishing time. Figure 11 shows the representative topographies of the surfaces after finishing through each of the four different process chains: DED+M1+MAF(Vf200), DED+M3+G1+MAF(Vf200), DED+M1+MAF(Vf1012), and DED+M3+G1+MAF(Vf1012). All surfaces were smoothed to a similar level regardless of the process chain. Nevertheless, changes in the roughness and skewness with time were noticeably different for process chain DED+M1+MAF with distinct feed rates. As the feed rate increased from 200 to 1012 mm/min, the particle brush tended to selectively remove the material from the peaks of surface undulations. This resulted in the greater reduction of roughness and skewness. In contrast, the faster magnet feed rate in the process chain (b) DED+M3+G1+MAF (1012 versus 200 mm/min) did not improve surface roughness as much as the other process chain (DED+M1+MAF). This can be associated with pit creation. Pit generation is inevitable in high-speed MAF. This is not only an MAF issue but a common one to loose-abrasive processes. Further studies on eliminating pit generation in high-speed polishing are essential to further extend the DED-produced part applications in the industry. The lower magnet feed rate (DED+M3+G1+MAF(Vf200)) completely altered ground surface (G1) to a MAF surface. This could have been because the ground surface in this chain was slightly smoother than that in MAF(Vf1012).

Figure 12 shows a topological map of the R_{sk} - R_{ku} values. Regarding kurtosis parameters (R_{ku}), mean R_{ku} values showed that the height distribution was spiked ($R_{ku} > 3$). Despite sample surface topography and roughness (R_a , R_z) after deposition and post-processes with different operations being totally different, the morphology of all surfaces is similar in terms of distribution of the peaks and valleys. The analysis of the R_{ku} parameter alone can lead to misinterpretation of surface topographic features. Therefore, the combined analysis of several parameters (i.e., R_a , R_z , R_{sk} , and R_{ku}) helps to properly interpret the surface profile. Regarding the skewness parameter (R_{sk}), while DEDed and milled samples showed positive R_{sk} values, ground and polished surfaces showed negative R_{sk} values. A positive degree of symmetry on the height distribution of peaks and valleys indicates profiles with high peaks or valleys filled in, while negative degrees indicate profiles with removed peaks or deep scratches [75]. Thus, a positive skewness ($R_{sk} > 0$) for the DED and milled samples can be associated by the presence of unmelted and partially melted powder particles adhered to the surface, as well as the feed marks generated by the cutting tool during machining, respectively. The negative skewness ($R_{sk} < 0$) for the ground and polished samples indicates surfaces had their peaks smoothed due to the interaction of

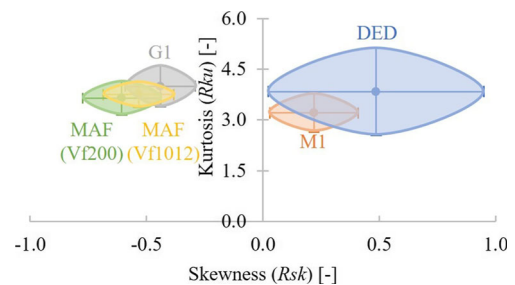
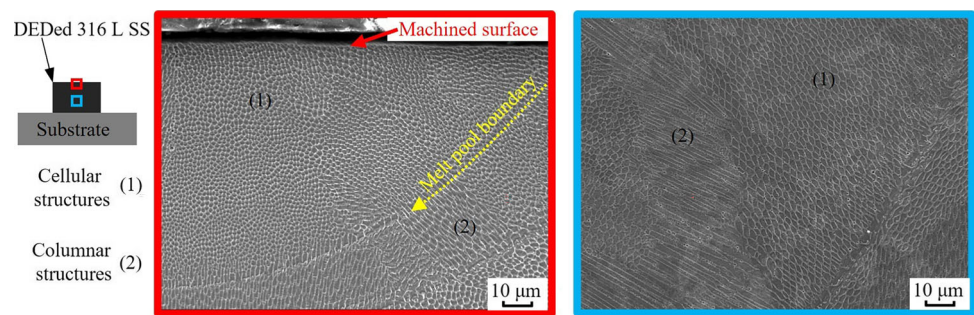


Fig. 12 R_{sk} - R_{ku} topological map of each respective process

Fig. 13 Microstructure of the cross-section DED+M1+MAF(Vf200) surface



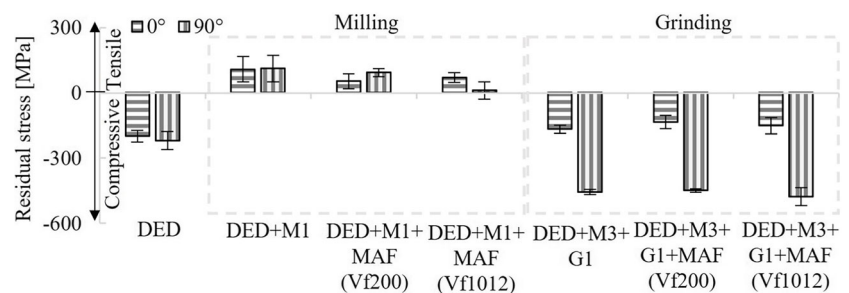
abrasive grains on the part surface, pointing to higher surface quality. Therefore, the surface shape left by DED can be altered through the application of post-processes. The high data dispersion of the DED samples was associated with the variability of the deposition process.

Figure 13 shows microstructures of the near-surface and centers of the DED workpieces after polishing. As shown in Fig. 6, columnar and equiaxial (cellular) structures are present in the workpiece, and these microstructures are commonly observed in DED-produced parts due to high cooling rates (from 10^3 to 10^5 Ks^{-1}) [27, 76]. Such microstructural components are similar to those reported by [77–79]. No major differences were seen between DED+M1+MAF and DED+M3+G1+MAF surfaces. Moreover, there were no major changes detected between structures near the surface and center of the workpieces, as shown in Fig. 13. This confirms that MAF is capable of smoothing the DED-produced workpieces with no observable changes in their microstructures. Moreover, no significant microstructural change was found (e.g., formation of white layer, burning, or cracks) near the milled/ground surfaces. Therefore, no near-surface microstructure alterations in the vicinity of the processes were observed. The 214 ± 6 HV microhardness obtained for all conditions remained statistically similar along the analyzed subsurface profile—ranging from 50 to 250 μm . Such values are similar to those reported by [80]. Thus, the microhardness in the subsurface region was also not affected by the milling/grinding/MAF processes for the tested conditions.

Figure 14 shows the residual stress (RS) of the surfaces after DED, milling, grinding, and MAF. The DEDed sample presents compressive RS, which is associated with the

temperature gradient of the melt pool (i.e., ΔT around the laser reduces the material strength and promotes the expansion of the layer, inducing compressive residual stress on the top surface layer) [81]. Such initial compressive stress state of DEDed-316 L SS is also reported by [82, 83]. This compressive state is associated with deposition parameters (i.e., laser power and feed rate). Future analysis of the residual stress depth-profile can indicate how the temperature gradient affects the stress distribution curves along with the interior of the part. The RS on the outer layer left by DED can be altered through the application of post-processes. Despite the fact that milled samples showed tensile RSs, ground surfaces showed compressive RSs. The parameters (e.g., cutting speed, feed, and depth of cut) and their effects (e.g., cutting forces and temperatures) are also responsible for this difference in the RS of milled and ground surfaces. Comparatively, the a_p used for milling was 0.4 mm, while for grinding, it was 0.01 mm, which can lead to higher heat generation for milled surfaces compared to ground samples. Milling induced a tensile RS on the top surface layer due to plastic deformation, thermal gradients, and metallurgic alterations in the subsurface structure (i.e., in the primary and secondary deformation zones during chip formation) [84]. On the other hand, grinding introduced compressive RS on the top surface layer due to inhomogeneous plastic deformation caused by the mechanical interaction of abrasive grains, thermal-plastic deformation, and phase transformation [85], with the former two being the main factors [86]. The compressive RS of ground samples is also an indicator of the cutting fluid efficiency, as high temperatures generate tensile RSs. Thus, changes in the tensile stress state of milled samples to

Fig. 14 Residual stresses for DEDed, milled, ground, and polished specimens



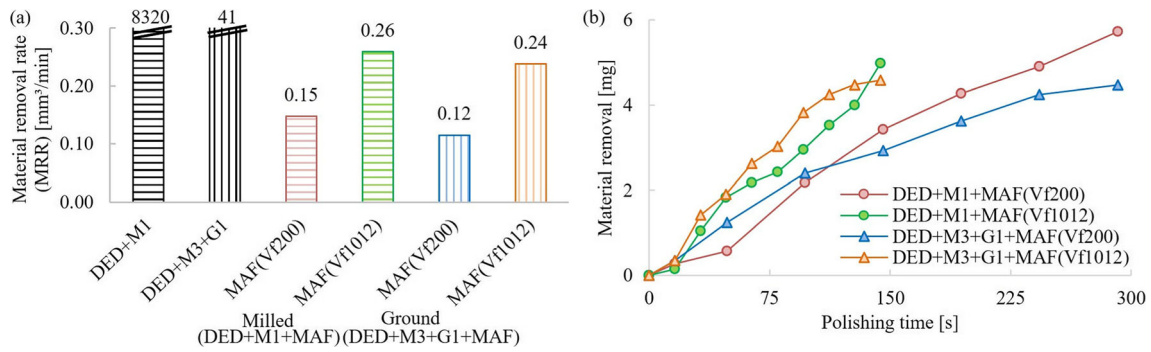


Fig. 15 **a** Material removal rate of each respective process and **b** material removal evolution of the samples under different polishing conditions

compressive RS after grinding positively affect mechanical proprieties, such as fracture resistance, corrosion resistance, and fatigue life. The MAF process does not change the RSs. The magnetic force (i.e., finishing force) acting on the iron particles is not enough to alter the subsurface structure (i.e., RS). For this purpose, iron particles should be replaced by magnetic spheres, as demonstrated by [28]. There is no significant difference between the RS values measured with the samples positioned at 0° and 90°, indicating no directionality of the results. This statement is not valid for ground samples (i.e., RS in the transverse direction, 0°, is different from those obtained in the grinding direction, 90°). This may be associated with the plastic deformation distributions in different directions over the ground surface, sliding-plowing actions, and the effects of part deformation and contraction levels in different directions (parallel and perpendicular to the wheel) [87].

4.2 Material removal rate, processing time, and specific energy

Figure 15a shows the material removal rate (MRR) of each post-process. Milling presented the highest material removal capacity (as mentioned in Sect. 2.1), up to 200 times higher than grinding. This behavior is explained by the high material removal in a short processing time compared to other post-processes. After MAF (see Fig. 15b), it was measured a material removal between 4.5 and 5.7 mg (for all polishing conditions), which is estimated to correspond to the removal of 2.3–3.5 μm in thickness. Ground samples showed less material removal during polishing when compared to milled ones. As such, the MAF process is more efficient for polishing rough surfaces. This can be associated with the abrasive grain behaviors in workpiece surface contact areas (ease of removal in the largest peaks and difficulty in accessing the bottom of the deepest valleys). MAF had the lowest MRRs, as is the nature of the polishing process. Nevertheless, polishing is fundamental for increasing

the surface quality of DEDed parts. A reduction of the polishing time (e.g., increasing the magnet feed rate) directly impacts MRR. The highest material removal rate is obtained in conditions in higher magnet feed rate conditions, with an advantage for the DED+M1+MAF(Vf1012) process chain. The active processing time for manufacturing surfaces with DED was 691.2 s in this process sequence, whereas t_c for M1 was 2.1 s in 3 passes, and MAF(Vf1012) required 128.1 s in 90 passes. Therefore, the entire processing sequence took 821.4 s (approximately 13.7 min), and the post-processing time was only 130.2 s. The DED+M3+G1+MAF(Vf1012) process chain took 9.5 s longer.

Figure 16 shows the regions of each post-process on the h_{eq} - u diagram, indicating the range of equivalent chip thickness (h_{eq}) and the specific energy (u) for each post-process. The h_{eq} value for milling was calculated according to Eq. 3, and h_{eq} values for grinding and polishing were according to Eq. 4. The calculated h_{eq} values for milling, grinding, and MAF were 74.3 μm, 2 nm, and 0.04–0.46 nm, respectively. Specific energy reduced as chip thickness increased. This is due to the cutting forces (machining power) and depth of cut involved in each process. The smaller those parameters, the smaller are the h_{eq} values, resulting in a scaling effect. As such, the values of energy spent for cutting are higher, while

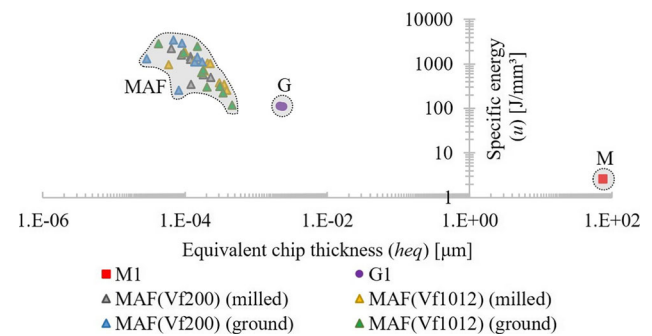


Fig. 16 Specific energy vs. equivalent chip thickness for M1, G1, and MAF

the energies related to plowing and sliding are lower. On the other hand, u increased as roughness was reduced. Regarding specific energy of the processes, milling (M1) resulted in lower u values (each pass consumed 3 ± 0.8 J/mm³) in order to achieve 1.55 ± 0.14 μm R_z (0.21 ± 0.02 μm R_a). Due to the cutting action of the abrasive grains, each grinding (G1) pass consumed 110 ± 2.8 J/mm³—about 42 times more energy compared to milling—reaching 1.16 ± 0.26 μm R_z (0.13 ± 0.03 μm R_a). The main purpose of the grinding process was to modify surface characteristics and improve surface quality. Thus, the process did not remove much material, and consequently, the removal rates implemented in this study (discussed above) are lower than the typical rates used in grinding. Likewise, h_{eq} values are also significantly lower. MAF has low-efficiency due to less material removal compared to other post-processes and the sliding-plowing ($u_{sl}-u_{pl}$) actions. Assuming that the specific cutting energy (u_c) is constant of 13.8 J/mm³ for steels [65], the ratio of u_c needed by the chip removal to u per pass is $2\pm 2\%$ in MAF (this value in accordance with the literature [88]). Thus, 98% of the energy is consumed for u_{sl} and u_{pl} in the case of DED-316L SS finishing. Comparatively, the ratio is 13% for grinding. Although a high u was spent during the polishing (1398 ± 933 J/mm³ in MAF(Vf200) and 955 ± 798 J/mm³ in MAF(Vf1012)) and a high u_{sl} ratio, the milling/grinding marks were smoothed, and the surface quality was improved— 0.55 ± 0.09 μm R_z and 0.06 ± 0.01 μm R_a in MAF(Vf200) and 0.67 ± 0.09 μm R_z and 0.08 ± 0.01 μm R_a in MAF(Vf1012). The u in MAF showed high data scattering due to the low material removal values per pass and the sensitivity of the material removal measurement.

Figure 17 shows the total specific energy of each process (calculated using Eqs. 2 and 1). Regarding milling and grinding, it is the sum of three passes. For MAF, it is the sum of 36 passes with a 200 mm/min feed rate and 90 passes with a 1012 mm/min feed rate. Note that the case with grinding under slow feed rate (DED+M3+G1+MAF(Vf200)) successfully smoothed the surface in shorter polishing time (129 s) (50%

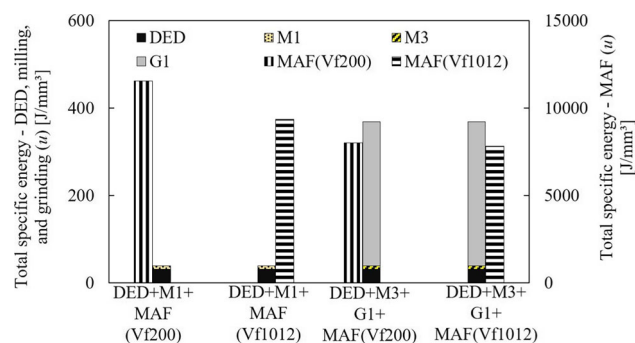


Fig. 17 Total specific energy of each respective process chain

of the time in the case without grinding (DED+M1+MAF(Vf200))). The total u for process chains DED+M1+MAF(Vf200), DED+M1+MAF(Vf1012), DED+M3+G1+MAF(Vf200), and DED+M3+G1+MAF(Vf1012) were 11611, 9390, 8373, and 8199 J/mm³, respectively. Thus, the selection of different process chains impacts not only the characteristics of the obtained surface but also the overall specific energy. MAF has a significant impact on the specific energy for all process chains (95.5–99.7%), and a reduction of the polishing time (e.g., increasing the magnet feed rate) has a direct impact on the overall specific energy. Because of the high level of specific energy in polishing, the impact of adding grinding on the overall specific energy was still small (330 J/mm³, corresponding to approximately 4% of the total). Nevertheless, adding grinding to the process chain reduced the overall specific energy needed to produce mirror-like surfaces, with energy being spent in the additional grinding steps instead.

Overall, this study highlights the significance of understanding manufacturing processes in tailoring effective post-processing techniques for achieving desired geometry and surface functionalities in AM-produced parts. Table 6 shows a summary of all results. In general, post-processing procedures brought changes to the surface characteristics of 316L stainless steel samples created through DED. Surface quality improved, as seen in reduced shape deviation and roughness, with no impact on microstructure and hardness. Moreover, grinding could shift residual stress from tension (post-milling) to compression, and MAF has minimal impact. Each operation had a specific material removal capacity, generating distinct cutting forces that influenced the specific cutting energy. This study also showed the feasibility of post-processing—from cutting to fine finishing—of DED parts using a machining center with one-time chucking. Nevertheless, the study does have some weaknesses: it exclusively examines flat surfaces, features low sensitivity in material removal measurements per MAF pass, and concentrates solely on the residual stress of the top surface. To address these limitations, future research could explore complex geometries, employ higher-resolution precision scales (such as 0.01 mg), and analyze residual stress profiles across varying depths, respectively.

5 Conclusions and outlooks

This study proposed a combined strategy of post-processing—from cutting to fine finishing—of 316L stainless steel parts made through DED using a machining center with one-time chucking. The main findings of this study are as follows:

Table 6 Summary of the main results of this study

Strategies adopted	DED	DED+M1	DED+M1+ MAF(Vf200)	DED+M1+ MAF(Vf1012)	DED+M3+ G1	DED+M3+G1+ MAF(Vf200)	DED+M3+G1+ MAF(Vf1012)	
Roughness	Rz (μm)	105.39	1.55	0.39	1.1	1.16	0.67	
	Rsk(μm)	0.49	0.22	−0.24	−0.2	−0.44	−0.96	
<p>The milled surface was rougher than the ground surface</p> <p>A positive skewness was obtained for milled surface, while negative skewness was obtained for the ground surface</p> <p>All surfaces were smoothed to a similar level regardless of the process chain</p> <p>As the feed rate increased from 200 to 1012 mm/min, the particle brush tended to selectively remove the material from the peaks of the surface undulations, resulting in the greater reduction of roughness and skewness</p>								
Microstructure and hardness	Cellular and columnar structures, 214 HV. No significant microstructural/hardness change was found near the milled/ground/polished surfaces							
Residual stress state	Compressive	Tensile			Compressive			
<p>While milled samples showed tensile residual stress, the ground surfaces showed compressive stress.</p> <p>The MAF process does not change the stress state</p>								
Total specific energy u (J/mm^3)	31	39	11,611	9,390	369	8,373	8,199	
<p>The ground samples showed less material removal during polishing when compared to the milled ones</p> <p>Milling resulted in lower specific energy values.</p> <p>Each grinding (G1) pass consumed about 42 times more energy compared to milling.</p> <p>MAF has a significant impact on the specific energy for all process chains (95.5–99.7%)</p>								

- The post-DED process chain of milling and grinding, followed by MAF, is capable of correcting surface errors of the produced parts with no observable changes in their near-surface microstructure and hardness. Nevertheless, the residual stress can be altered through the application of post-processes. With the conditions used, milling induced tensile residual stress, while grinding introduced compressive residual stress. The effect of MAF on residual stress was not as significant as milling and grinding.
- Grinding and MAF processes have demonstrated successful integration into vertical machining centers, offering the possibility of concurrent utilization within a single apparatus for post-processing DED-316L with one-time chucking. As such, the precise selection of appropriate grinding wheels, dressing techniques, cooling mechanisms, and fixation systems becomes pivotal in ensuring the attainment of satisfactory grinding outcomes. In the case of MAF, the magnetic field and forces, magnetic pole geometry, and spindle rotation are all intricate technical prerequisites that exert a transformative influence on the

flexible brush, thereby directly impacting the interactions among magnetic particles on the specimen’s surface. This, in turn, significantly affects the polishing efficacy. Hence, the careful choice of those attributes becomes imperative, contingent upon the specific material removal conditions and surface geometry parameters (including shape accuracy, roughness, and surface texture) as stipulated during the design phase of the fabricated component.

- The equivalent chip thickness in polishing is one hundredth of its thickness in grinding and one millionth in milling. Polishing took up most of the processing time and specific energy. A post-DED process chain with a reduced polishing time helps reduce both.
- Conventional grinding wheels permit the utilization of static dressers featuring a single tip, fliesen, or conglomerate design (easily installable within machining centers), yielding components manufactured via DED with micro-level roughness. The adoption of superabrasive wheels, in contrast to conventional ones, presents a potential

avenue for enhancing material removal rates, albeit at the expense of surface quality. Nevertheless, the implementation of effective dressing systems (such as laser, touch dressing, and rotary dressers) becomes imperative to modulate the aggressiveness of the grinding wheel. This modulation, in turn, offers the prospect of augmenting the surface quality of the resulting components. However, for each of these alternatives, the incorporation of peripheral and ancillary systems into the machinery becomes indispensable, necessitating substantial technological and economic resources.

- While grinding consumes approximately 42 times more specific energy than milling, and MAF expends 10 times more specific energy than grinding, abrasive processes play a fundamental role in producing components with superior surface quality. This, in turn, enhances the longevity, durability, and overall functionality of the product. For instance, when considering the application of 316L stainless steel in the biomedical field, surface roughness significantly influences the mechanisms governing the osseointegration of implants, as well as corrosion resistance.
- Grinding enabled the removal of milling marks; thus, the DED part surface processed with milling followed by grinding showed negative skewness and lower roughness than surfaces processed with milling only. As a result, grinding slightly reduced the material removal rate in polishing but helped reduce the time needed for polishing and the overall specific energy.
- High-speed MAF accomplished by increasing the spindle rotational speed and feed rate is feasible, and this significantly contributes to the increased material removal rate and overall reduction of specific energy. Nevertheless, an excessive increase in the particle-brush rotational speed reduces the number of particles engaged with the work-piece surface, diminishing polishing performance. This factor limits the improvement of the process-chain efficiency.

As future proposals:

- Understanding the characteristics of each process helps post-AM manufacturing process choices that impart desired surface functions, in addition to producing desired geometries. Studying the effects of post-AM processing on physical/mechanical properties (e.g., corrosion, wear, fatigue strength) is critical to improving the overall reliability of AM parts. This fundamental study (only flat surfaces were studied) will serve as a basis for future work involving complex geometries and/or internal channels that are difficult to access using traditional manufacturing processes. Additional investigations will

be conducted in order to reduce the processing time for finishing AM part surfaces.

Acknowledgements The authors would like to thank the following companies: Blaser Swisslube do Brasil Ltda, Materials Institute of Brazil (MIB), and Saint-Gobain Abrasives.

Funding This work was supported by the Fundação de Amparo à Pesquisa do Estado de São Paulo (FAPESP) (Grant numbers 2016/11309-0 and 2019/10758-4) and the Conselho Nacional de Desenvolvimento Científico e Tecnológico (CNPq).

Declarations

Conflict of interest The authors declare no competing interests.

References

1. Sundgren JE, Bodö P, Lundström I, Berggren A, Hellem S (1985) Auger electron spectroscopic studies of stainless-steel implants. *J Biomed Mater Res* 19(6):663–671. <https://doi.org/10.1002/jbm.820190606>
2. Peuster M, Hesse C, Schloo T, Fink C, Beerbaum P, von Schnakenburg C (2006) Long-term biocompatibility of a corrodible peripheral iron stent in the porcine descending aorta. *Biomaterials* 27(28):4955–4962. <https://doi.org/10.1016/j.biomaterials.2006.05.029>
3. Lou X, Song M, Emigh PW, Othon MA, Andresen PL (2017) On the stress corrosion crack growth behaviour in high temperature water of 316L stainless steel made by laser powder bed fusion additive manufacturing. *Corros Sci* 128:140–153. <https://doi.org/10.1016/j.corsci.2017.09.017>
4. Song M, Wang M, Lou X, Rebak RB (2019) Was GS Radiation damage and irradiation-assisted stress corrosion cracking of additively manufactured 316L stainless steels. *J Nucl Mater* 513:33–44. <https://doi.org/10.1016/j.jnucmat.2018.10.044>
5. Adair ST, Attwood PA (2014) In-service stress corrosion cracking of AISI 316L stainless steel in an H2S environment. *Corros Eng Sci Technol* 49(5):396–400. <https://doi.org/10.1179/1743278213Y.0000000141>
6. Faille C, Membre JM, Tissier JP, Bellon-Fontaine MN, Carpentier B, Laroche MA, Benezech T (2000) Influence of physicochemical properties on the hygienic status of stainless steel with various finishes. *Biofouling* 15(4):261–274. <https://doi.org/10.1080/08927010009386317>
7. Jullien C, Bénézech T, Carpentier B, Leuret V, Faille C (2002) Identification of surface characteristics relevant to the hygienic status of stainless steel for the food industry. *J Food Eng* 56(1):77–87. [https://doi.org/10.1016/S0260-8774\(02\)00150-4](https://doi.org/10.1016/S0260-8774(02)00150-4)
8. Ibrahim MZ, Sarhan AA, Yusuf F, Hamdi M (2017) Biomedical materials and techniques to improve the tribological, mechanical and biomedical properties of orthopedic implants - a review article. *J Alloys Compd* 714:636–667. <https://doi.org/10.1016/j.jallcom.2017.04.231>
9. Axinte D, Guo Y, Liao Z, Shih AJ, M'Saoubi R, Sugita N (2019) Machining of biocompatible materials - recent advances. *CIRP Annals* 68(2):629–652. <https://doi.org/10.1016/j.cirp.2019.05.003>
10. Breme H, Biehl V, Reger N, Gawalt E (2016) Handbook of biomaterial properties, 2nd edn. Springer, New York, Ch. Chapter 1a - Metallic Biomaterials: Introduction, pp 151–158. <https://doi.org/10.1007/978-1-4939-3305-1>

11. DebRoy T, Wei HL, Zuback JS, Mukherjee T, Elmer JW, Milewski JO, Beese AM, Wilson-Heid A, De A, Zhang W (2018) Additive manufacturing of metallic components - process, structure and properties. *Prog Mater Sci* 92:112–224. <https://doi.org/10.1016/j.pmatsci.2017.10.001>
12. Mahale RS, Shamanth V, Hemanth K, Nithin SK, Sharath PC, Shashanka R, Patil A, Shetty D (2022) Processes and applications of metal additive manufacturing. *Mater Today Proc* 54:228–233. <https://doi.org/10.1016/j.matpr.2021.08.298>
13. Kok Y, Tan XP, Wang P, Nai ML, Loh NH, Liu E, Tor SB (2018) Anisotropy and heterogeneity of microstructure and mechanical properties in metal additive manufacturing: a critical review. *Mater Des* 139:565–586. <https://doi.org/10.1016/j.matdes.2017.11.021>
14. Thompson SM, Bian L, Shamsaei N, Yadollahi A (2015) An overview of direct laser deposition for additive manufacturing; Part I: Transport phenomena, modeling and diagnostics. *Addit Manuf* 8:36–62. <https://doi.org/10.1016/j.addma.2015.07.001>
15. Svetlizky D, Das M, Zheng B, Vyatskikh AL, Bose S, Bandyopadhyay A, Schoenung JM, Lavernia EJ, Eliaz N (2021) Directed energy deposition (DED) additive manufacturing: physical characteristics, defects, challenges and applications. *Mater Today* 49:271–295. <https://doi.org/10.1016/j.mattod.2021.03.020>
16. Ahn DG, Lee HJ, Cho JR, Guk DS (2016) Improvement of the wear resistance of hot forging dies using a locally selective deposition technology with transition layers. *CIRP Ann Manuf Technol* 65(1):257–260. <https://doi.org/10.1016/j.cirp.2016.04.013>
17. Hofmann DC, Kolodziejska J, Roberts S, Otis R, Dillon RP, Suh JO, Liu ZK, Borgonia JP (2014) Compositionally graded metals: a new frontier of additive manufacturing. *J Mater Res* 29(17):1899–1910. <https://doi.org/10.1557/jmr.2014.208>
18. Ansari M, Jabari E, Toyserkani E (2021) Opportunities and challenges in additive manufacturing of functionally graded metallic materials via powder-fed laser directed energy deposition: a review. *J Mater Process Technol* 294. <https://doi.org/10.1016/j.jmatprotec.2021.117117>
19. Saboori A, Aversa A, Marchese G, Biamino S, Lombardi M, Fino P (2019) Application of directed energy deposition-based additive manufacturing in repair. *Applied Sciences (Switzerland)* 9(16). <https://doi.org/10.3390/app9163316>
20. Bennett J, Garcia D, Kendrick M, Hartman T, Hyatt G, Ehmann K, You F, Cao J (2018) Repairing automotive dies with directed energy deposition: industrial application and life cycle analysis. *J Manuf Sci Eng, Trans ASME* 141(2). <https://doi.org/10.1115/1.4042078>
21. Yamazaki T (2016) Development of a hybrid multi-tasking machine tool: integration of additive manufacturing technology with CNC machining. *Procedia CIRP* 42:81–86. <https://doi.org/10.1016/j.procir.2016.02.193>
22. Liu G, Du D, Wang K, Pu Z, Zhang D, Chang B (2017) High-temperature oxidation behavior of a directionally deposited. *Corros Sci* 193. <https://doi.org/10.1016/j.corsci.2021.109918>
23. Zhou Z, Lei Q, Yan Z, Wang Z, Shang Y, Li Y, Qi H, Jiang L, Liu Y, Huang L (2021) Effects of process parameters on microstructure and cracking susceptibility of a single crystal superalloy fabricated by directed energy deposition. *Mater Des* 198. <https://doi.org/10.1016/j.matdes.2020.109296>
24. Aydogan B, O'Neil A, Sahasrabudhe H (2021) Microstructural and mechanical characterization of stainless steel 420 and Inconel 718 multi-material structures fabricated using laser directed energy deposition. *J Manuf Process* 68:1224–1235. <https://doi.org/10.1016/j.jmapro.2021.06.031>
25. Rai AK, Srinivasulu B, Paul CP, Singh R, Rai SK, Mishra GK, Bontha S, Bindra KS (2020) Development of thick sic coating on thin wall tube of zircaloy-4 using laser based directed energy deposition technique. *Surf Coat Technol* 398. <https://doi.org/10.1016/j.surfcoat.2020.126088>
26. Bajaj P, Hariharan A, Kini A, Kürnsteiner P, Raabe D, Jäggle EA (2020) Steels in additive manufacturing: a review of their microstructure and properties. *Mater Sci Eng A* 772. <https://doi.org/10.1016/j.msea.2019.138633>
27. Gibson I, Rosen D, Stucker B (2015) Additive manufacturing technologies 3D printing, rapid prototyping, and direct digital manufacturing, 2nd edn. Springer. <https://doi.org/10.1007/978-1-4939-2113-3>
28. Yamaguchi H, Fergani O, Wu PY (2017) Modification using magnetic field-assisted finishing of the surface roughness and residual stress of additively manufactured components. *CIRP Ann Manuf Technol* 66(1):305–308. <https://doi.org/10.1016/j.cirp.2017.04.084>
29. Greco S, Kieren-Ehse S, Kirsch B, Aurich JC (2021) Micro milling of additively manufactured AISI 316L: impact of the layerwise microstructure on the process results. *Int J Adv Manuf Technol* 112(1–2):361–373. <https://doi.org/10.1007/s00170-020-06387-3>
30. Garthe KU, Hoyer KP, Hagen L, Tillmann W, Schaper M (2021) Correlation between pre- and post-treatments of additively manufactured 316L parts and the resulting low cycle fatigue behavior. *Rapid Prototyp J* 28(5):833–840. <https://doi.org/10.1108/RPJ-01-2021-0017>
31. Dabwan A, Anwar S, Al-Samhan AM, Alfaify A, Nasr MM (2021) Investigations on the effect of layers' thickness and orientations in the machining of additively manufactured stainless steel 316L. *Materials* 14(7). <https://doi.org/10.3390/ma14071797>
32. Iqbal AS, Amri SE, Shrestha S, Wang Z, Manogharan GP, Bukkapatnam S (2017) Longitudinal milling and fine abrasive finishing operations to improve surface integrity of metal AM components. *Procedia Manuf* 10:990–996. <https://doi.org/10.1016/j.promfg.2017.07.090>
33. Yazdanpanah A, Lago M, Gennari C, Dabalà M (2021) Stress corrosion cracking probability of selective laser melted 316L austenitic stainless steel under the effect of grinding induced residual stresses. *Metals* 11(2):1–20. <https://doi.org/10.3390/met11020327>
34. Chang S, Liu A, Ong CYA, Zhang L, Huang X, Tan YH, Zhao L, Li L, Ding J (2019) Highly effective smoothing of 3D-printed metal structures via overpotential electrochemical polishing. *Mater Res Lett* 7(7):282–289. <https://doi.org/10.1080/21663831.2019.1601645>
35. Wu PY, Hirtler M, Bambach M, Yamaguchi H (2020) Effects of build- and scan-directions on magnetic field-assisted finishing of 316L stainless steel disks produced with selective laser melting. *CIRP J Manuf Sci Technol* 31:583–594. <https://doi.org/10.1016/j.cirpj.2020.08.010>
36. Spierings AB, Starr TL, Wegener K (2013) Fatigue performance of additive manufactured metallic parts. *Rapid Prototyp J* 19(2):88–94. <https://doi.org/10.1108/13552541311302932>
37. Mesicek J, Ma QP, Hajnys J, Zelinka J, Pagac M, Petru J, Mizera O (2021) Abrasive surface finishing on SLM 316L parts fabricated with recycled powder. *Appl Sci (Switzerland)* 11(6). <https://doi.org/10.3390/app11062869>
38. Kirsch B, Hotz H, Hartig J, Greco S, Zimmermann M, Aurich JC (2020) Pendulum and creep feed grinding of additively manufactured AISI 316L. *Procedia CIRP* 101:166–169. <https://doi.org/10.1016/j.procir.2020.03.156>
39. Rotty C, Mandroyan A, Doche ML, Hihn JY (2016) Electropolishing of CuZn brasses and 316L stainless steels: influence of alloy composition or preparation process (ALM vs. standard method). *Surf Coat Technol* 307:125–135. <https://doi.org/10.1016/j.surfcoat.2016.08.076>
40. Zhang J, Wang H (2022) Magnetically driven internal finishing of AISI 316L stainless steel tubes generated by laser powder bed

- fusion. *J Manuf Process* 76:155–166. <https://doi.org/10.1016/j.jmapro.2022.02.009>
41. Liu C, Yan D, Tan J, Mai Z, Cai Z, Dai Y, Jiang M, Wang P, Liu Z, Li CC, Lao C, Chen Z (2020) Development and experimental validation of a hybrid selective laser melting and CNC milling system. *Addit Manuf* 36:101550. <https://doi.org/10.1016/j.addma.2020.101550>
 42. Blinn B, Greco S, Smaga M, Zimmermann M, Hotz H, Müller D, Hartig J, Kirsch B, Aurich JC, Beck T (2021) Influence of microstructural defects and the surface topography on the fatigue behavior of “additively-subtractively” manufactured specimens made of AISI 316L. *Mater Werkst* 52(5):561–577. <https://doi.org/10.1002/mawe.202000266>
 43. Wu PY, Yamaguchi H (2018) Material removal mechanism of additively manufactured components finished using magnetic abrasive finishing. *Procedia Manuf* 26:394–402. <https://doi.org/10.1016/j.promfg.2018.07.047>
 44. Chen L, Richter B, Zhang X, Bertsch KB, Thoma DJ, Pfefferkorn FE (2021) Effect of laser polishing on the microstructure and mechanical properties of stainless steel 316L fabricated by laser powder bed fusion. *Mater Sci Eng A* 802:140579. <https://doi.org/10.1016/j.msea.2020.140579>
 45. Bruzzo F, Catalano G, Demir AG, Previtali B (2021) Surface finishing by laser re-melting applied to robotized laser metal deposition. *Opt Lasers Eng* 137. <https://doi.org/10.1016/j.optlaseng.2020.106391>
 46. Amanov A (2020) Effect of local treatment temperature of ultrasonic nanocrystalline surface modification on tribological behavior and corrosion resistance of stainless steel 316L produced by selective laser melting. *Surf Coat Technol* 398:126080. <https://doi.org/10.1016/j.surfcoat.2020.126080>
 47. Alharbi N (2022) Shot peening of selective laser-melted SS316L with ultrasonic frequency. *Int J Adv Manuf Technol* 119(3–4):2285–2299. <https://doi.org/10.1007/s00170-021-08398-0>
 48. Zhang C, Chen F, Huang Z, Jia M, Chen G, Ye Y, Lin Y, Liu W, Chen B, Shen Q, Zhang L, Lavernia EJ (2019) Additive manufacturing of functionally graded materials: a review. *Mater Sci Eng A* 764. <https://doi.org/10.1016/j.msea.2019.138209>
 49. Sugavaneswaran M, Jebaraj AV, Kumar MD, Lokesh K, Rajan AJ (2018) Enhancement of surface characteristics of direct metal laser sintered stainless steel 316L by shot peening. *Surf Interfaces* 12:31–40. <https://doi.org/10.1016/j.surf.2018.04.010>
 50. Kaynak Y, Kitay O (2019) The effect of post-processing operations on surface characteristics of 316L stainless steel produced by selective laser melting. *Addit Manuf* 26:84–93. <https://doi.org/10.1016/j.addma.2018.12.021>
 51. An L, Wang D, Zhu D (2022) Combined electrochemical and mechanical polishing of interior channels in parts made by additive manufacturing. *Addit Manuf* 51:102638. <https://doi.org/10.1016/j.addma.2022.102638>
 52. Wang B, Castellana J, Melkote SN (2021) A hybrid post-processing method for improving the surface quality of additively manufactured metal parts. *CIRP Annals* 70(1):175–178. <https://doi.org/10.1016/j.cirp.2021.03.010>
 53. Melia MA, Duran JG, Koepke JR, Saiz DJ, Jared BH, Schindelholz EJ (2020) How build angle and post-processing impact roughness and corrosion of additively manufactured 316L stainless steel. *NPJ Materials Degradation* 4(1):1–11. <https://doi.org/10.1038/s41529-020-00126-5>
 54. Tyagi P, Goulet T, Riso C, Stephenson R, Chuenprateep N, Schlitzer J, Benton C, Garcia-Moreno F (2019) Reducing the roughness of internal surface of an additive manufacturing produced 316 steel component by chempolishing and electropolishing. *Addit Manuf* 25:32–38. <https://doi.org/10.1016/j.addma.2018.11.001>
 55. Masek P, Fornusek T, Zeman P, Bucko M, Smolik J, Heinrich P (2019) Machinability the AISI 316 stainless steel after processing by various methods of 3D printing. *MM Science Journal* 2019:3338–3346. <https://doi.org/10.17973/MMSJ.2019112019091>
 56. Gong Y, Li P (2019) Analysis of tool wear performance and surface quality in post milling of additive manufactured 316L stainless steel. *J Mech Sci Technol* 33(5):2387–2395. <https://doi.org/10.1007/s12206-019-0237-x>
 57. Coelho R, Azevedo R, Assis C (2018) An investigation of anisotropy on AISI 316L obtained by additive manufacturing (AM) measuring surface roughness after micro-endmilling operations. In: European society for precision engineering and nanotechnology (EUSPEN), conference proceedings - 18th international conference and exhibition pp 357–358
 58. Morimoto Y, Kato H, Hasegawa A, Takasugi K, Stein M, Yamaguchi H (2018) Combination of non-axisymmetric curved surface turning and magnetic abrasive finishing. *Int Symp Flex Auto*, pp 296–301
 59. Heng L, Kim YJ, Mun SD (2017) Review of superfinishing by the magnetic abrasive finishing process. *High Speed Machining* 3(1):42–55. <https://doi.org/10.1515/hsm-2017-0004>
 60. Soshi M, Ring J, Young C, Oda Y, Mori M (2017) Innovative grid molding and cooling using an additive and subtractive hybrid CNC machine tool. *CIRP Ann Manuf Technol* 66(1):401–404. <https://doi.org/10.1016/j.cirp.2017.04.093>
 61. Flynn JM, Shokrani A, Newman ST, Dhokia V (2016) Hybrid additive and subtractive machine tools - research and industrial developments. *Int J Mach Tools Manuf* 101:79–101. <https://doi.org/10.1016/j.ijmactools.2015.11.007>
 62. Yang Y, Gong Y, Li C, Wen X, Sun J (2021) Mechanical performance of 316 L stainless steel by hybrid directed energy deposition and thermal milling process. *J Mater Process Technol* 291:117023. <https://doi.org/10.1016/j.jmatprotec.2020.117023>
 63. Bourell D, Kruth JP, Leu M, Levy G, Rosen D, Beese AM, Clare A (2017) Materials for additive manufacturing. *CIRP Ann Manuf Technol* 66(2):659–681. <https://doi.org/10.1016/j.cirp.2017.05.009>
 64. Maleki E, Bagherifard S, Bandini M, Guagliano M (2021) Surface post-treatments for metal additive manufacturing: progress, challenges, and opportunities. *Addit Manuf* 37. <https://doi.org/10.1016/j.addma.2020.101619>
 65. Malkin S, Guo C (2008) Grinding technology: theory and applications of machining with abrasives, 2nd edn. Industrial Press, New York
 66. Wegener K, Hoffmeister HW, Karpuschewski B, Kuster F, Hahmann WC, Rabiey M (2011) Conditioning and monitoring of grinding wheels. *CIRP Annals - Manuf Technol* 60(2):757–777. <https://doi.org/10.1016/j.cirp.2011.05.003>
 67. Guo J, Au KH, Sun CN, Goh MH, Kum CW, Liu K, Wei J, Suzuki H, Kang R (2019) Novel rotating-vibrating magnetic abrasive polishing method for double-layered internal surface finishing. *J Mater Process Technol* 264:422–437. <https://doi.org/10.1016/j.jmatprotec.2018.09.024>
 68. Teng X, Zhang G, Zhao Y, Cui Y, Li L, Jiang L (2019) Study on magnetic abrasive finishing of AISi10Mg alloy prepared by selective laser melting. *Int J Adv Manuf Technol* 105(5–6):2513–2521. <https://doi.org/10.1007/s00170-019-04485-5>
 69. Zou Y, Xie H, Zhang Y (2020) Study on surface quality improvement of the plane magnetic abrasive finishing process. *Int J Adv Manuf Technol* 109(7–8):1825–1839. <https://doi.org/10.1007/s00170-020-05759-z>
 70. Matweb (2022) Online materials information resource. <http://www.matweb.com>
 71. Simchi A (2006) Direct laser sintering of metal powders: mechanism, kinetics and microstructural features. *Mater Sci Eng A* 428(1–2):148–158. <https://doi.org/10.1016/j.msea.2006.04.117>

72. Ståhl JE, Schultheiss F (2012) Analytical calculation of the true equivalent chip thickness for cutting tools and its influence on the calculated tool life. *Adv Mater Res* 576:80–86. <https://doi.org/10.4028/www.scientific.net/AMR.576.80>
73. AMERICAN SOCIETY FOR TESTING AND MATERIALS (2017) ASTM E384 - 17: standard test method for microindentation hardness of materials. <https://doi.org/10.1520/E0384-17>
74. Noyan IC, Cohen JB (1987) *Residual stress: measurement by diffraction and interpretation*, 1st edn. Springer Science+Business Media, New York. <https://doi.org/10.1007/978-1-4613-9570-6>
75. Gadelmawla ES, Koura MM, Maksoud TM, Elewa IM, Soliman HH (2002) Roughness parameters. *J Mater Process Technol* 123(1):133–145. [https://doi.org/10.1016/S0924-0136\(02\)00060-2](https://doi.org/10.1016/S0924-0136(02)00060-2)
76. Zheng B, Zhou Y, Smugeresky JE, Schoenung JM, Lavernia EJ (2008) Thermal behavior and microstructural evolution during laser deposition with laser-engineered net shaping: Part I. Numerical calculations. *Metall Mater Trans A: Phys Metall Mater Sci* 39(9):2228–2236. <https://doi.org/10.1007/s11661-008-9557-7>
77. Ma M, Wang Z, Zeng X (2017) A comparison on metallurgical behaviors of 316L stainless steel by selective laser melting and laser cladding deposition. *Mater Sci Eng A* 685:265–273. <https://doi.org/10.1016/j.msea.2016.12.112>
78. Saboori A, Piscopo G, Lai M, Salmi A, Biamino S (2020) An investigation on the effect of deposition pattern on the microstructure, mechanical properties and residual stress of 316L produced by directed energy deposition. *Mater Sci Eng A* 780. <https://doi.org/10.1016/j.msea.2020.139179>
79. Guo D, Yan K, Callaghan MD, Daisenberger M, Chatterton J, Chen J, Wisbey A, Mirihanage W (2021) Solidification microstructure and residual stress correlations in direct energy deposited type 316L stainless steel. *Mater Des* 207:109782. <https://doi.org/10.1016/j.matdes.2021.109782>
80. Yu J, Rombouts M, Maes G (2013) Cracking behavior and mechanical properties of austenitic stainless steel parts produced by laser metal deposition. *Mater Des* 45:228–235. <https://doi.org/10.1016/j.matdes.2012.08.078>
81. Mercelis P, Kruth JP (2006) Residual stresses in selective laser sintering and selective laser melting. *Rapid Prototyp J* 12(5):254–265. <https://doi.org/10.1108/13552540610707013>
82. Piscopo G, Salmi A, Atzeni E (2021) Influence of high-productivity process parameters on the surface quality and residual stress state of AISI 316L components produced by directed energy deposition. *J of Materi Eng and Perform* 30(9):6691–6702. <https://doi.org/10.1007/s11665-021-05954-3>
83. Kumaran M, Senthilkumar V, Justus Panicke CT, Shishir R (2021) Investigating the residual stress in additive manufacturing of repair work by directed energy deposition process on SS316L hot rolled steel substrate. *Mater Today Proc* 47:4475–4478. <https://doi.org/10.1016/j.matpr.2021.05.319>
84. El-Khabeery MM, Fattouh M (1989) Residual stress distribution caused by milling. *Int J Mach Tools Manuf* 29(3):391–401. [https://doi.org/10.1016/0890-6955\(89\)90008-4](https://doi.org/10.1016/0890-6955(89)90008-4)
85. Ding W, Zhang L, Li Z, Zhu Y, Su H, Xu J (2017) Review on grinding-induced residual stresses in metallic materials. *Int J Adv Manuf Technol* 88(9–12):2939–2968. <https://doi.org/10.1007/s00170-016-8998-1>
86. Zhang LC, Suto T, Noguchi H, Waida T (1992) An overview of applied mechanics in grinding. *Manuf Rev* 5(4):261–273. <https://www.precision-manufacturing.unsw.edu.au>
87. Balart MJ, Bouzina A, Edwards L, Fitzpatrick ME (2004) The onset of tensile residual stresses in grinding of hardened steels. *Mater Sci Eng A* 367(1–2):132–142. <https://doi.org/10.1016/j.msea.2003.10.239>
88. Hashimoto F, Yamaguchi H, Krajnik P, Wegener K, Chaudhari R, Hoffmeister HW, Kuster F (2016) Abrasive fine-finishing technology. *CIRP Ann Manuf Technol* 65(2):597–620. <https://doi.org/10.1016/j.cirp.2016.06.003>

Publisher's Note Springer Nature remains neutral with regard to jurisdictional claims in published maps and institutional affiliations.

Springer Nature or its licensor (e.g. a society or other partner) holds exclusive rights to this article under a publishing agreement with the author(s) or other rightsholder(s); author self-archiving of the accepted manuscript version of this article is solely governed by the terms of such publishing agreement and applicable law.